



NTNU – Trondheim
Norwegian University of
Science and Technology

Investigation of Heat Storage in Future Wood Stoves

Kristin Sveine Ytredal

Master of Science in Mechanical Engineering

Submission date: February 2015

Supervisor: Erling Næss, EPT

Co-supervisor: Kolbeinn Kristjansson, EPT

Norwegian University of Science and Technology
Department of Energy and Process Engineering

EPT-M-2014- 155

MASTEROPPGAVE

for

Student Kristin Sveine Ytredal

Høsten 2014

Undersøkelse av varmelagring i fremtidens vedovner

*Investigation of heat storage in future woodstoves***Bakgrunn og målsetting**

Institutt for Energi- og Prosesseteknikk er involvert i forskning og utvikling av neste generasjons vedovner. Ett av målene for slike vedovner er at de skal ha en jevnere varmeeffektavgivelse enn dagens ovner. Dette krever at man benytter et varmelager sammen med ovnen. For å oppnå høy energilagringstetthet er det fordelaktig å benytte et faseovergangsmateriale (PCM, Phase Change Material) som varmelagringsmedium. PCM-materialer har generelt ikke egenskaper som er fordelaktige i varmelagre som skal reagere raskt på påført varme, da de har lav termisk konduktivitet og degraderer ved temperaturer som oppnås ved bruk av vedovner. Ved å øke den effektive termiske konduktiviteten kan man redusere problemene med overoppheting samt oppnå god varmedistribusjon.

For å forbedre den effektive termiske konduktiviteten i et PCM materiale kan man eksempelvis benytte finner eller metallskum. Et testoppsett for å måle temperaturresponsen til et PCM system (med mulighet for finner/skum) er bygd ved NTNU. Dette oppsettet skal brukes til å teste effekten av ulike forbedringsmetoder for termisk konduktivitet.

Opgaven er en videreføring av prosjektarbeidet.

Oppgaven bearbeides ut fra følgende punkter

1. Varmeavgivelse fra et PCM varmelager og til omgivelsene skal studeres. Dette innebærer etablering av en beregningsmodell som inkluderer de aktuelle varmetransportmekanismene, samt utarbeidelse av en egnet geometri som best mulig sikrer en jevn effektavgivelse. Dimensjonerende effektavgivelse skal bestemmes i samarbeid med instituttet. Beregningsmodellen(e) skal presenteres, og resultatene diskuteres.
2. Det skal gjennomføres eksperimentelle målinger på et eksisterende forsøksoppsett for PCM varmelagre. Formålet er å bestemme den effektive termiske konduktiviteten i varmelageret, samt netto varmelagringskapasitet. Et måleprogram skal etableres i samarbeid med instituttet. Resultatene skal presenteres og sammenliknes med resultater fra numeriske beregninger. Det skal gjennomføres en usikkerhetsanalyse for den målte termiske konduktiviteten.

3. Basert på resultatene fra oppgavens pkt. 1 og 2 skal en komplett beregningsmodell for varmetilførsel, lagring og varmeavgivelse fra et PCM varmelager med en gitt varmeavgivelsesprofil fra en vedovn utarbeides. I den grad tiden tillater skal modellen benyttes til å optimalisere ytelsen for et PCM varmelager for en gitt varmeavgivelsesprofil for en vedovn.
4. Det skal utarbeides forslag til videre arbeid.

Senest 14 dager etter utlevering av oppgaven skal kandidaten levere/sende instituttet en detaljert fremdrift- og eventuelt forsøksplan for oppgaven til evaluering og eventuelt diskusjon med faglig ansvarlig/veiledere. Detaljer ved eventuell utførelse av dataprogrammer skal avtales nærmere i samråd med faglig ansvarlig.

Besvarelsen redigeres mest mulig som en forskningsrapport med et sammendrag både på norsk og engelsk, konklusjon, litteraturliste, innholdsfortegnelse etc. Ved utarbeidelsen av teksten skal kandidaten legge vekt på å gjøre teksten oversiktlig og velskrevet. Med henblikk på lesning av besvarelsen er det viktig at de nødvendige henvisninger for korresponderende steder i tekst, tabeller og figurer anføres på begge steder. Ved bedømmelsen legges det stor vekt på at resultatene er grundig bearbeidet, at de oppstilles tabellarisk og/eller grafisk på en oversiktlig måte, og at de er diskutert utførlig.

Alle benyttede kilder, også muntlige opplysninger, skal oppgis på fullstendig måte. For tidsskrifter og bøker oppgis forfatter, tittel, årgang, sidetall og eventuelt figurnummer.

Det forutsettes at kandidaten tar initiativ til og holder nødvendig kontakt med faglærer og veileder(e). Kandidaten skal rette seg etter de reglementer og retningslinjer som gjelder ved alle (andre) fagmiljøer som kandidaten har kontakt med gjennom sin utførelse av oppgaven, samt etter eventuelle pålegg fra Institutt for energi- og prosesssteknikk.

Risikovurdering av kandidatens arbeid skal gjennomføres i henhold til instituttets prosedyrer. Risikovurderingen skal dokumenteres og inngå som del av besvarelsen. Hendelser relatert til kandidatens arbeid med uheldig innvirkning på helse, miljø eller sikkerhet, skal dokumenteres og inngå som en del av besvarelsen. Hvis dokumentasjonen på risikovurderingen utgjør veldig mange sider, leveres den fulle versjonen elektronisk til veileder og et utdrag inkluderes i besvarelsen.

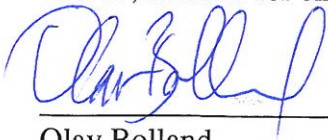
I henhold til "Utfyllende regler til studieforskriften for teknologistudiet/sivilingeniørstudiet" ved NTNU § 20, forbeholder instituttet seg retten til å benytte alle resultater og data til undervisnings- og forskningsformål, samt til fremtidige publikasjoner.

Besvarelsen leveres digitalt i DAIM. Et faglig sammendrag med oppgavens tittel, kandidatens navn, veileders navn, årstall, institutt navn, og NTNUs logo og navn, leveres til instituttet som en separat pdf-fil. Etter avtale leveres besvarelse og evt. annet materiale til veileder i digitalt format.

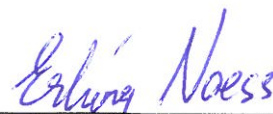
Arbeid i laboratorium (vannkraftlaboratoriet, strømnings teknisk, varmeteknikk)

Feltarbeid

NTNU, Institutt for energi- og prosesssteknikk, 27. august 2014



Olav Bolland
Instituttleder



Erling Næss
Faglig ansvarlig/veileder

Medveileder: Ph.d.-student Kolbeinn Kristjansson, NTNU

Preface

This master's thesis presents a research performed at the Norwegian University of Science and Technology (NTNU), Department of Energy and Process Engineering.

The aim of this research was to investigate the development of the new generation wood stoves adapted to energy efficient buildings by adopting new solutions that will combine heat supply, storage and distribution in an optimal way.

This work would never been accomplished without the help and contributions received from others. I am sincerely grateful to my supervisor and co-supervisor, Erling Næss and Kolbeinn Kristjansson for all help, support and guidance.

Trondheim, 25 February 2015

Kristin Sveine Ytredal

Abstract

The objective of this work was to investigate heat storage in a heat storage unit utilizing a phase change material (PCM). This included finding an optimal geometry for heat transfer from the heat storage unit to the surroundings, finding an effective thermal conductivity of the PCM, and combine these in an overall PCM heat storage model. The advantage of using a PCM is that the PCM can store large amounts of heat in liquid phase as latent heat. This will contribute to a stable heat release to the surroundings.

Methods for enhancing the heat transfer from a PCM heat storage unit to the surroundings were studied. The research considered both free convection and radiation heat transfer. Further objectives were to find a suitable geometry of fins for heat rejection to the surroundings. Heat transfer from two different fin arrangements to the surroundings were investigated, a fin array and fin channels. The dimensions of the geometries were optimized. Both geometries showed satisfying results, but it was concluded that fin channels were preferable to a fin array.

A heat storage unit was investigated experimentally. The experiments considered two different setups, supplying heat to the heat storage units top surface, and supplying heat to the bottom surface. The results were compared to results from numerical simulations. The heat storage unit heated from the top surface showed good agreement compared to results from numerical simulations. The heat storage unit heated from below proved that heat transfer by free convection in the liquid phase had a significant impact on the melting pace of the PCM. The comparison with results from numerical simulations did however not show an immediate agreement.

The effective thermal conductivity of the PCM was found based on the experiments and compared to literature values. An uncertainty analysis was performed on the obtained effective conductivity. The results showed that the method employed for studying the effective conductivity was inaccurate.

An overall heat storage model was developed to combine heat supply, heat storage and heat distribution. The simulations were performed using PCM as well as PCM with aluminium foam to enhance the heat distribution in the heat storage unit and the heat transfer rate to the surroundings. The heat supplied to the heat storage unit was based

on calculations of batch combustion of wood. The results showed that none of the tests for the PCM heat storage unit, or the optimization of the PCM heat storage unit, reached the requirements of heat transfer to the surroundings set for the model. The length of the PCM heat storage unit was also proved to be excessive.

Sammendrag

Målet for dette arbeidet var å undersøke varmelagring i et varmelager som benytter et faseendringsmateriale (phase change material, PCM). Arbeidet innebar å finne en optimal geometri for varmeoverføring fra varmelageret til omgivelsene. En effektiv termisk konduktivitet for PCM ble også funnet. Disse funnene ble kombinert i en komplett PCM varmelagrings modell. Fordelen med å bruke et faseendringsmateriale i kombinasjon med en vedovn er at et faseendringsmateriale kan lagre store mengder varme i flytende fase som latent varme. Dette vil bidra til en mer stabil og jevn varmeavgivelse til omgivelsene.

Metoder for forbedring av varmeoverføring fra et PCM varmelager til omgivelsene ble studert. Studien tar for seg varmetransport med både frikonveksjon og stråling. En av oppgavene var å finne en egnet finnegeometri som best mulig sikrer en jevn effektavgivelse til omgivelsene. Varmeoverføring fra to ulike finnegeometrier til omgivelsene ble undersøkt og dimensjonene deres optimalisert. Begge geometriene viste gode resultater, men det ble bestemt at finnekanalen var det beste valget.

Det ble gjennomført eksperimentelle målinger på et PCM varmelager. Forsøkene testet to forskjellige oppsett hvor varme ble tilført varmelageret fra topp, og fra bunn. Resultatene ble sammenlignet med resultater fra numeriske beregninger. Varmelageret som ble varmet fra topp viste gode resultater sammenlignet med resultater fra numeriske beregninger. Resultatene fra varmelageret som ble varmet fra bunn viste at varmeoverføring ved frikonveksjon i væskefasen har en betydelig innvirkning på smeltetempoet til faseendringsmaterialet. Resultatene ble sammenlignet med resultater fra numeriske beregninger, men disse viste imidlertid ikke noen umiddelbar overenstemmelse.

Den effektive termiske konduktiviteten til faseendringsmaterialet ble bestemt på grunnlag av forsøkene og sammenlignet med litteraturverdier. En usikkerhetsanalyse ble gjennomført for den målte termiske konduktiviteten. Resultatene viste at metoden som benyttes for å bestemme den effektive konduktiviteten var unøyaktig.

En komplett beregningsmodell for varmetilførsel, lagring og varmeavgivelse fra et PCM varmelager ble utarbeidet. Et varmeavgivelsesprofil fra en vedovn ble brukt som varmetilførsel. Simuleringene ble utført for PCM og PCM med aluminiumskum. Ved å bruke aluminiumskum sammen med et PCM kan man forbedre varmefordelingen i materialet og

varmeoverføringen til omgivelsene. Resultatene viste at ingen av testene for PCM varme-
lager eller optimalisering av PCM-lageret oppnådde de krav som stilles til varmeoverføring
fra varmelageret, og lengden på lageret ble vist å være overdreven.

Notation

A	area, (m ²)
A_c	cross-sectional area, (m ²)
C_p	specific heat capacity, (kJ/kgK)
D_h	hydraulic diameter, (m)
G	irradiation, (W/m ²)
g	gravitational force, (m/s ²)
Gr	Grashof number
H	fin height, (m)
H_{sl}	latent heat, (kJ/kg)
h	convection heat transfer coefficient, (W/mK)
J	radiosity, (W/m ²)
k	thermal conductivity, (W/m ² K)
L	characteristic length, (m)
\dot{m}	mass flow, (kg/s)
Nu	Nusselt number
NTU	number of transfer units
P	perimeter, (m)
p	pressure, (N/m ²)
Pr	Prandtl number
Q	heat transfer rate, (W)
q	heat flux, (W/m ²)
Ra	Rayleigh number
Re	Reynolds number
S	fin spacing, (m)
T	temperature, (K)
x_c	critical location for transition to turbulence, (m)

Greek symbols

α	thermal diffusivity, (m ² /s)
β	volumetric thermal expansion coefficient, (K ⁻¹)
ε	porosity; heat exchanger effectiveness
η	similarity variable
η_f	fin efficiency
μ	viscosity, (kg/sm)
ν	kinematic viscosity, (m ² /s)
ρ	density, (kg/m ³)
σ	Stefan-Boltzmann constant

Subscripts

amb	ambient
b	base
<i>c</i>	cross-sectional; cold fluid
ch	channel
conv	convection
eff	effective
<i>f</i>	fluid; fin
h	hot fluid
<i>L</i>	characteristic length
<i>l</i>	liquid
lm	log mean condition
m	mean value, mutual
max	maximum
por	porous media
rad	radiation
<i>s</i>	solid
sur	surroundings

Table of contents

Preface	iii
Abstract	v
Sammendrag	vii
Notation	ix
List of figures	xvi
List of tables	xviii
1 Introduction	1
1.1 Background	1
1.2 Objectives	2
1.3 Structure	2
2 Literary review	3
2.1 Introduction	3
2.2 Fin arrays	4
2.3 Pin fin arrays	5
2.4 Effect of radiation on free convection heat transfer	6
3 Heat rejection model	9
3.1 Fin geometry	9
3.1.1 Dimensions and effect requirements	10
3.2 Fin array	11
3.2.1 Boundary layer calculation for a vertical plate	11
3.2.2 Parallel plate channels	12
3.2.3 Numerical simulations	13
3.2.4 Results and discussion – fin array	15
3.3 Fin channel	17
3.3.1 Mass flow for the vertical channel	17

xi

TABLE OF CONTENTS

3.3.2	Heat transfer from free convection and radiation	20
3.3.3	Total heat transfer	21
3.3.4	Fin efficiency	22
3.3.5	Total heat transfer considering fin efficiency	23
3.3.6	Results and discussion – fin channel	24
3.4	Summary, conclusions and discussion	27
4	Heat storage study	29
4.1	Introduction	29
4.2	Test rig	30
4.3	Heat storage unit heated from the top	32
4.3.1	Numerical model - heat storage unit heated from the top	33
4.4	Heat storage unit heated from below	34
4.4.1	Numerical model – heat storage unit heated from below	34
4.5	Results and discussion	36
4.5.1	Heat storage unit heated from the top	36
4.5.2	Heat storage unit heated from below	38
4.6	Thermal conductivity	39
4.7	Uncertainty analysis	41
4.8	Summary, conclusions and discussion	43
5	Overall PCM heat storage model	45
5.1	Heat supply, storage and distribution	45
5.2	Numerical model and boundary conditions	46
5.3	PCM	49
5.4	PCM with aluminium foam	50
5.5	Results and discussion	51
5.5.1	Heat storage unit heated with one batch of wood	51
5.5.2	Heat storage unit heated with two batches of wood	54
5.5.3	Optimisation of the PCM heat storage unit	56
5.6	Summary, conclusions and discussion	61
6	Summary, conclusions and recommendations	63
6.1	Summary and conclusions	63
6.2	Recommendations for further work	65
	Bibliography	67

Appendix	69
A Data	69
A.1 Material properties	69
A.2 Material properties of erythritol with aluminium foam with a porosity of 95%	71
B Net heat storage capacity	73
C Uncertainty analysis	75
C.1 Uncertainties	76
C.2 Conductivity of solid erythritol	76
C.3 Liquid conductivity:	
Experiment heated from the top	77
C.4 Liquid conductivity:	
Experiment heated from below	79
D Risk assessment	81

TABLE OF CONTENTS

List of Figures

- 2.1 Fin configuration geometry of Yazicioğlu and Yüncü [14] 4
- 2.2 Investigated orientations of pin-fin arrays of Sparrow and Vemuri [11] 5
- 2.3 Assembly of fins showing 18-fin and 68-fin arrays [11] 6

- 3.1 The two different fin geometries investigated. 10
- 3.2 Fin array and cross-sectional area with dimensions. 11
- 3.3 Comsol model with boundary conditions. 14
- 3.4 Heat flux for different fin heights with $T_s = 393$ K. 15
- 3.5 Fin channel and cross-sectional area with dimensions. 17
- 3.6 Fin channel used for calculations 18
- 3.7 Length from base to tip of the fin. 22
- 3.8 Heat flux for $H = 15$ mm for different surface temperatures. 24
- 3.9 Heat flux for $H = 15$ mm for different surface temperatures. 25
- 3.10 Fin efficiency for a fin height of $H = 15$ mm with $T_s = 393$ K. 25
- 3.11 Heat flux for $H = 15$ mm for different surface temperatures. 26

- 4.1 Experimental setup. 30
- 4.2 Positioning of thermocouples TT01 to TT09 inside the heat storage. 31
- 4.3 PCM heat storage unit heated from the top. 32
- 4.4 Setup of PCM heat storage unit heated from the top modeled using Comsol. 33
- 4.5 PCM heat storage unit heated from the top, with boundary conditions shown. 33
- 4.6 PCM heat storage unit heated from below with compressed air system. . . 34
- 4.7 Sketch of Comsol model for experiment heated from below. 35
- 4.8 Measured temperatures in the storage unit for thermocouples TT01 to TT09. 36
- 4.9 Temperature of each thermocouple from Comsol compared to experiment . 37
- 4.10 Comparison of melting front for experiments and numerical model 38
- 4.11 Thermal conductivity of liquid erythritol to average relative error. 40
- 4.12 Effective thermal conductivity of liquid erythritol from experiment with curve-fit. 41

- 5.1 Sketch of a PCM heat storage unit mounted with a fin arrangement. 46

LIST OF FIGURES

5.2	PCM heat storage unit with hot and cold surfaces.	46
5.3	Heat flux from the wood stove supplied to the PCM heat storage unit. . .	47
5.4	Heat flux from two batches of wood supplied to the PCM heat storage unit.	47
5.5	Heat transfer coefficient used as boundary condition on cold surface of heat storage unit.	48
5.6	Effective thermal conductivity of liquid erythritol	49
5.7	Melting front position in a storage unit heated with one batch of wood. . .	51
5.8	Temperature at hot surface for a storage unit heated with one batch of wood.	52
5.9	Heat flux for a storage unit heated with one batch of wood.	52
5.10	Temperature at cold surface for a storage unit heated with one batch of wood.	53
5.11	Melting front position in a storage unit utilizing PCM with aluminium foam, heated with two batches of wood.	54
5.12	Temperature at hot surface for a storage unit utilizing PCM with alu- minium foam, heated with two batches of wood.	54
5.13	Heat flux for a storage unit utilizing PCM with aluminium foam, heated with two batches of wood.	55
5.14	Temperature at cold surface for a storage unit utilizing PCM with alu- minium foam, heated with two batches of wood.	55
5.15	Melting front for a storage unit with a length of 50 mm.	56
5.16	Temperature at hot surface for a storage unit with a length of 50 mm. . . .	57
5.17	Heat flux for a storage unit with a length of 50 mm.	57
5.18	Temperature at cold surface for a storage unit with a length of 50 mm. . .	58
5.19	Melting front for two heat storage units with a length of 100 mm and 50 mm.	58
5.20	Temperature at hot surface for two heat storage units with a length of 100 mm and 50 mm.	59
5.21	Heat flux for two heat storage units with a length of 100 mm and 50 mm. .	59
5.22	Temperature at cold surface for two heat storage units with a length of 100 mm and 50 mm.	60

List of Tables

3.1	Temperature boundary conditions for fin array in Comsol	14
3.2	Built-in material properties of aluminium from Comsol.	15
3.3	Nusselt numbers and friction factors for fully developed laminar flow in tubes of rectangular cross-sectional area (p. 519 in [5]).	18
4.1	Actual position of thermocouples inside the heat storage unit.	32
4.2	Material properties of erythritol employed in Comsol.	34
4.3	Material properties of erythritol employed in Comsol.	35
4.4	Net heat storage capacity found using Comsol	37
4.5	Thermal conductivity of solid erythritol determined using Hot Disk	39
4.6	Thermal conductivity of liquid erythritol found from experiment with storage unit heated from the top.	40
4.7	Uncertainty of conductivity of solid erythritol obtained using Hot Disk.	42
4.8	Uncertainty of conductivity of liquid erythritol obtained from experiment with storage unit heated from the top.	42
4.9	Average uncertainty of effective thermal conductivity of liquid erythritol obtained from experiment with storage unit heated from below.	42
A.1	Material properties of teflon	69
A.2	Material properties of silcapor	69
A.3	Material properties of Erythritol	70
A.4	Material properties of aluminum [5]	71
A.5	Properties of erythritol including aluminium foam with a porosity of 95%	72
B.1	Net heat storage capacity found using Comsol	73
B.2	Net heat storage capacity from calculations	74
C.1	Uncertainties	76
C.2	Uncertainty of solid erythritol	77
C.3	Nominal values and individual uncertainties for q_s	77
C.4	Individual uncertainties of liquid conductivity from black box	78
C.5	Uncertainty of liquid conductivity	78

LIST OF TABLES

C.6	Measured nominal values for different time steps	79
C.7	Individual uncertainties for liquid conductivity measurements	80
C.8	Uncertainty and average uncertainty of liquid conductivity	80

Chapter 1

Introduction

1.1 Background

This master's thesis is part of a study involving research and development of the next generation wood stoves adapted to energy efficient buildings. The study is a continuation of project work conducted during the spring of 2014 [15].

New houses and buildings as well as upgrading of old houses have increased the focus on improved insulation to reduce the heat loss to the air outside. This will set new demands for the heating, as the requirement for heating will be reduced. Most wood stoves used today produce more heat than needed for modern houses. To achieve a more stable heat release and distribution new solutions must be developed that will combine heat supply, storage and distribution in an optimum way that current solutions and technologies cannot offer [12].

A more stable heat release can be achieved with a heat storage unit containing a phase change material (PCM) used in combination with a wood stove. The advantage of using a PCM is that the material can store large amounts of heat by melting and solidification. When heat is added to the material, the material will keep its temperature constant at the melting temperature of the PCM, and the heat is stored as latent heat, this will contribute to an even heat release [8].

This work will mainly focus on the investigation of heat storage in a PCM heat storage unit and heat release from the unit to the surroundings. To ensure that the heat transferred from the heat storage unit to the surroundings will fulfill the required rate of heat transfer, fins are added to the surface to increase the surface area, thereby enhancing the heat transfer rate. To improve the heat distribution inside the storage unit aluminium foam is added to the PCM. This will enhance the thermal conductivity of the PCM and cause increased heat storage. The study was performed using experimental and numerical

methods. The numerical simulations were performed using Comsol Multiphysics.

1.2 Objectives

The overall objective of this study is to investigate heat storage in a PCM heat storage unit and heat release to the surroundings. This includes the study of a heat distribution concept for heat transfer from a PCM heat storage unit to the surroundings. Based on this, a calculation model including the different heat transfer modes will be developed, where the aim is to achieve an optimum fin geometry for an even heat release.

Experiments will be performed on a heat storage unit utilizing PCM. The experiments will measure the temperatures of the gradually melting PCM in the storage unit. The aim of the experiments is to determine the effective thermal conductivity of the PCM and net heat storage capacity. An uncertainty analysis will be conducted on the measured thermal conductivity. The results obtained from the experiments will be compared to results from numerical simulations.

An overall numerical model considering heat supply to the heat storage unit, heat storage and heat release to the surroundings will be developed. The optimum fin geometry and the effective thermal conductivity will be implemented in the model. The simulations will include PCM as well as PCM with aluminium foam for enhanced heat transfer. A heat flux based on calculations of batch combustion of wood is supplied to the model. The heat storage unit is to be optimized to meet the requirements for heat transfer.

1.3 Structure

This thesis consists of six chapters and is organized as follows. Chapter 1 presents an introduction and describes the basis for this thesis. Chapter 2 gives a brief introduction to a literature review concerning heat transfer to the surroundings with natural convection and radiation for different fin geometries and arrangements. Chapter 3 describes an investigation on finding an optimized heat distribution concept for heat transfer to the surroundings, where two different fin geometries were studied. Chapter 4 describes the experiments that were carried out. The results from the experiments were compared to results from numerical simulations. An uncertainty analysis has been carried out on the effective thermal conductivity found for the PCM. Chapter 5 presents an overall numerical model considering heat supply to the heat storage unit, heat storage and heat rejection to the surroundings. The study is carried out using a model for PCM compared to a model including PCM with aluminium foam. Finally, Chapter 6 presents a summary and recommendations for further work.

Chapter 2

Literary review

2.1 Introduction

Increasing the heat transfer coefficient or the surface area of a geometry can enhance the heat transfer from that surface. The use of extended surfaces like fins is often more economical, convenient and trouble free. Most devices requiring enhanced heat transfer add fins to the surface to increase the surface area, and thereby they achieve the required rate of heat transfer. However, adding fins to a surface will require an optimization of the fin spacing since adding numerous fins will increase the surface area and it can affect the heat transfer rate negatively because of resistance to the air flow or causing of boundary layer interference [14]. Heat distribution from a finned system to the surroundings can be obtained by using the principles of convection and radiation heat transfer. Radiation contribution to the total heat transfer rate is quite low due to low emissivity values of commonly used fin materials, such as aluminum alloys. Experimental data found for free convection is generally less precise and accurate than for forced convection, owing to the slower rates of heat transfer and the associated difficulty of taking measurements without disturbing the process [4].

Several varieties of fin geometries and arrangements have been studied in the literature, and typical fin analysis can be found in several textbooks [6]. This literary review will mainly focus on heat transfer with natural convection and radiation for different fin geometries and arrangements and to what extent different fin arrangements could improve heat transfer from a surface to the surroundings.

2.2 Fin arrays

Güvenç and Yüncü [3] performed an experimental investigation on performance of fin arrays. The investigation considered a vertical base with free convection heat transfer. They tested several different fin configurations where the main objective of their study was to obtain an optimum fin geometry for maximum performance of the fin array. They wanted to investigate the effects the geometric parameters such as fin height, fin spacing and base-to-ambient temperature difference had on the heat transfer performance of the fin arrays. They showed that fin spacing is the most significant parameter in the performance of fin arrays, and for every fin height and base to ambient temperature difference there exists an optimum value of fin spacing. Higher heat transfer enhancement was obtained with vertically oriented fins than with horizontally oriented fins for fin arrays of the same geometry. They compared their results to heat transfer from a vertical plate with no fins, showing that for all fin arrays the convective heat transfer rate was higher than for the vertical plate. Their overall conclusion was that heat transfer from an array depends strongly on the geometry of the fin array, fin height and fin spacing.

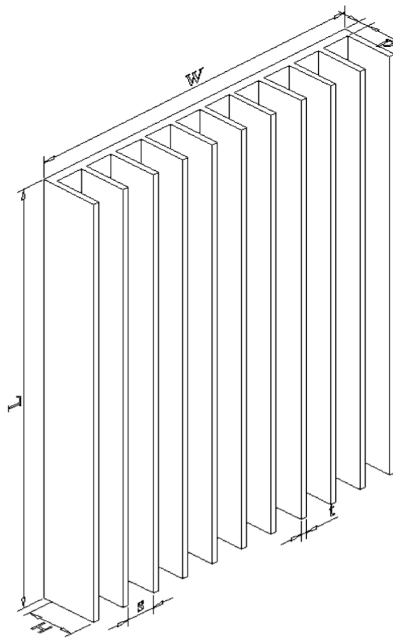


Figure 2.1: Fin configuration geometry of Yazicioğlu and Yüncü [14]

Yazicioğlu and Yüncü [14] investigated experimentally heat transfer from aluminum fins. Figure 2.1 shows the fin configuration they used. The investigation was performed to extend the data obtained from Güvenç and Yüncü, using the same experimental setup and method. They performed numerous experiments on different geometries of the fin array. Their conclusions were the same as for Güvenç and Yüncü. For a given base to ambient temperature difference, the convective heat transfer rate from fin arrays takes on a

maximum value as a function of fin spacing, which maximizes the convective heat transfer rate from the fin array. The results show that the convective heat transfer rate from fin arrays depends on fin height, fin length, fin spacing and base-to-ambient temperature difference.

2.3 Pin fin arrays

Mueller and Abu-Mulaweh [6] performed measurements of the temperature along a fin cooled by natural convection and radiation. They considered a horizontal pin-fin with cylindrical cross sectional area where one end of the fin was maintained at a constant temperature. The objective of the study was to predict the temperature in a long horizontal pin-fin using a local heat transfer coefficient that accounted for both natural convection and radiation. A comparison was made to experimental results and the agreement was good. Their results showed that heat loss due to radiation was significant and must be taken into consideration.

Sparrow and Vemuri [11] investigated three different orientations of pin fin arrays, see Figure 2.2 and Figure 2.3. The three different orientations were (a) horizontal fins on a vertical baseplate, (b) vertical fins on a horizontal down facing baseplate and (c) vertical fins on a horizontal upfacing baseplate. The experiments were performed in air and measured the combined natural convection and radiation heat transfer. They discovered that when they increased the number of fins while holding all the other parameters at fixed values the heat transfer rates would first increase reaching a maximum and thereby decreasing, defining an optimum fin configuration. They found that the vertical upfacing fin array yielded the highest heat transfer rates, followed by the horizontal fin array and the vertical down facing fin array.

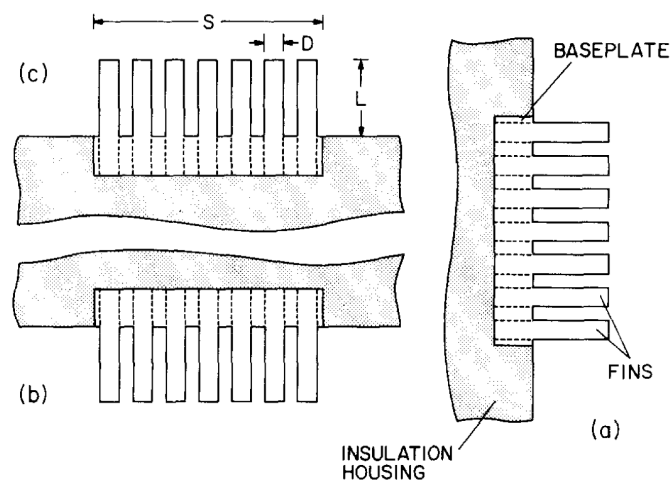


Figure 2.2: Investigated orientations of pin-fin arrays of Sparrow and Vemuri [11]

Sparrow and Vemuri used a configuration of multiple pin fins on a base plate as seen in Figure 2.3, and for three different orientations, compared to Güvenç and Yüncü, and Yazicioğlu and Yüncü, who tested different numbers of fins along a vertical base plate in one direction (see Figure 2.1). When they increased the number of fins the heat transfer rate would first increase reaching a maximum and thereby decreasing, defining an optimum. They all achieved good results, and similar behaviour of the heat transfer rate. Although Güvenç and Yüncü [3], and Yazicioğlu and Yüncü [14] performed the experiments taking only the convective heat transfer effects into account.

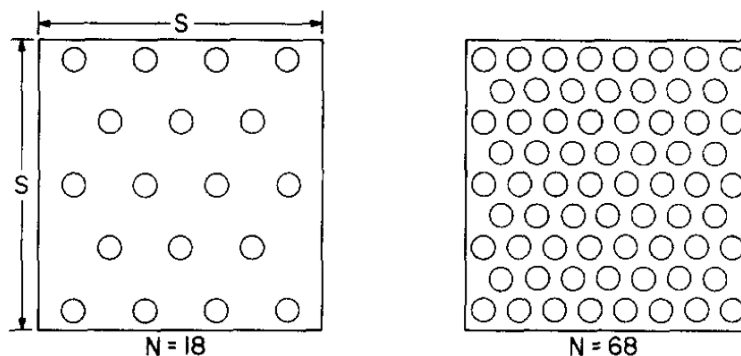


Figure 2.3: Assembly of fins showing 18-fin and 68-fin arrays [11]

2.4 Effect of radiation on free convection heat transfer

Natural convection in air is generally accompanied by radiation heat transfer. For a finned system that is essentially isothermal, the natural convection and radiation heat transfer are decoupled and are additive. This is the case if the radiation or the free convection heat transfer is so small that it does not affect the fin efficiency [11].

Rammohan Rao and Venkateshan [10] investigated experimentally and numerically the interaction of free convection and radiation in horizontal fin arrays. Their results showed the effects of changing parameters such as emissivity of the fin surface, fin spacing, fin height and base temperature. They also studied some of the earlier literature on this topic to look at the coupling between radiation and free convection, as they thought this coupling had not received the attention it deserved.

In most studies fin arrays are often considered isothermal. This assumption would be reasonable assumptions for short fins with small fin spacing made of materials of high conductivity. For tall fins however, the assumption of an isothermal surface is not always justified. The temperature variation in fins is an interaction between the conduction of the fin material, as well as natural convection and radiation of the fin surface. Rammohan Rao and Venkateshan investigation concluded that all previous studies assuming an isothermal

fin surface had overestimated the radiative as well as the convective heat transfer. This means that the interaction between radiation and convection invalidates the additive approach based on the assumption of decoupled free convection and radiation [10].

This literature review shows that there are many experimental and numerical investigations concerning heat transfer from fin geometry and arrangements. Not all of the above mentioned have considered radiation heat transfer in their experiments, although several have concluded that heat transfer due to radiation from fin arrays are significant.

Chapter 3

Heat rejection model

3.1 Fin geometry

When firing up in a wood stove the effect from the stove will increase rapidly resulting in a high release of heat. Using a PCM heat storage unit combined with a wood stove will ensure that the effect peaks will be reduced, causing a lower amount of heat rejected to the surroundings over a longer period of time. To ensure that the heat transferred from the heat storage unit to the surroundings will fulfill the required rate of heat transfer, fins are added to the surface to increase the surface area enhancing the heat transfer rate. Chapter 2 presents a brief literature review on heat transfer from different fin geometries and arrangements. On this basis a study has been carried out to find an optimized heat distribution concept using fins.

A flat plate without fins has proved not to be sufficient for achieving the required heat transfer. A first approach to the problem is to investigate heat transfer from a simple fin array. Güvenç and Yüncü [3], and Yazicioğlu and Yüncü [14] received good agreement with their experimental study; their study form the basis of the comparison of this study. A second approach is to close off the fin array using a thin plate, creating an array of multiple fin channels of rectangular cross sectional area. This will create a chimney effect for heat transfer enhancement. It will also be a more esthetic choice of geometry for wood stoves used in housing. Figure 3.1 shows the two different fin arrangements to be optimized and investigated.

There was established a calculation model for heat distribution from the PCM heat storage unit to the surroundings. The effectiveness of the fin is enhanced by the choice of a material of high thermal conductivity. The fin material used in this study is therefore aluminium. Heat transfer to air by natural convection and radiation is considered. Theory and data from Incropera et al. [5] form the basis of all calculations performed, where most

material properties are calculated using "table-lookup" interpolation. For the calculations a Matlab computer code was developed and numerical simulations were performed using Comsol Multiphysics.

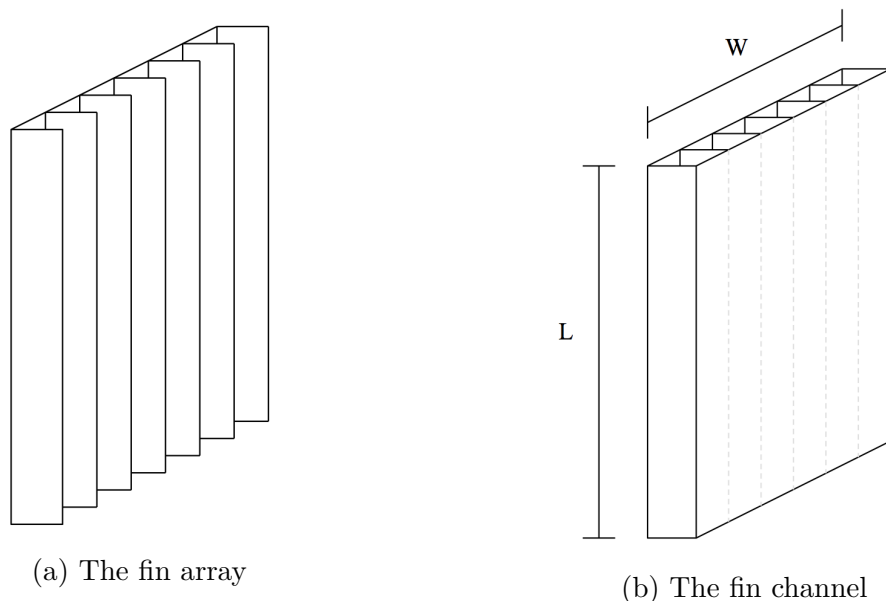


Figure 3.1: The two different fin geometries investigated.

3.1.1 Dimensions and effect requirements

A wood stove with a total heat transfer rate of 4.5 kW will form the basis for this study. It is assumed that half of the heat will be delivered to the room from the wood stove through glass doors/windows in the stove. The other half is delivered to the PCM heat storage unit. The heat transfer rate from the storage unit to the surroundings is determined to be 600 W.

Three out of four of the wood stoves vertical surfaces will be supplied with a PCM heat storage unit of equal surface area. The base surfaces will be quadratic, with a length (L) and width (W) of 0.3 m and a surface area of 0.09 m². The total surface area of the base will then be 0.27 m². As seen from Equation 3.1 below, this will require a heat release of approximately 2200 W/m² from the PCM heat storage unit to the surroundings. As the dimensions of the base is set, the variables to be optimized are the fin height and fin spacing.

$$q = \frac{600\text{W}}{0.27\text{m}^2} \approx 2200\text{W/m}^2 \quad (3.1)$$

3.2 Fin array

A study was performed on a fin array with a vertical base, where the fins are of constant cross sectional area. The study was inspired by the experiments performed by Güvenç and Yüncü [3], and Yazicioğlu and Yüncü [14] presented in Section 2.2. Figure 3.2 shows the dimensions of the geometry and cross-sectional area of the fin array. When calculating heat transfer from the fin surface both natural convection and radiation heat transfer was considered. As the surface area of the base was already decided, variables to be optimized were the fin height (H) and fin spacing (S). The study was carried out using empirical equations from Incropera et al. [5] and Comsol Multiphysics.

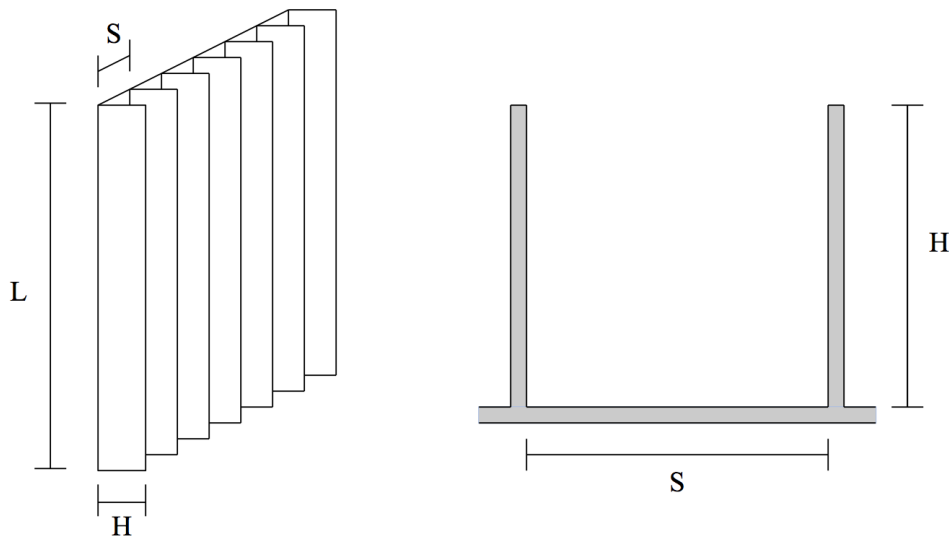


Figure 3.2: Fin array and cross-sectional area with dimensions.

3.2.1 Boundary layer calculation for a vertical plate

For vertical channels the buoyancy forces will act to develop motion causing boundary layers to develop on each surface. For long channels of fin arrays with small spacing boundary layers developing on opposing surfaces will eventually merge to yield a fully developed condition. Calculations determining the free convection boundary layer is therefore necessary (p. 566 – 570 in [5]). Considering a vertical plate the Grashof number is

$$\text{Gr}_L = \frac{g\beta(T_s - T_\infty)L^3}{\nu^2} \quad (3.2)$$

From the Grashof number the flow can be considered laminar or turbulent using the critical Rayleigh number for vertical plates

$$\text{Ra}_{x,c} = \text{Gr}_{x,c} \text{Pr} = \frac{g\beta(T_s - T_\infty)x^3}{\nu\alpha} \approx 10^9 \quad (3.3)$$

A similarity solution to the foregoing problem has been obtained. The solution involves transforming variables by introducing a similarity parameter of the form

$$\eta \equiv \frac{y}{x} \left(\frac{\text{Gr}_x}{4} \right)^{1/4} \quad (3.4)$$

From Figure 9.4a in [5], for fully developed velocity profile for a flat plate, $y \approx \delta$. Hence

$$\delta_L \approx \frac{\eta L}{(\text{Gr}_L/4)^{1/4}} \quad (3.5)$$

Where η is found from Figure 9.4a in [5] for different Prandtl numbers.

The solution shows that boundary layer thickness are typically larger for free convection than for forced convection [5]. Results from these calculations show that if the fin arrays are closer spaced than 4.4 cm the boundary layer will merge to a fully developed laminar condition. The equations from the following Section 3.2.2 will therefore apply. The reader is requested to see reference for more details regarding calculations.

3.2.2 Parallel plate channels

From boundary layer calculations the results showed that two fins spaced closer than 4.4 cm will cause a fully developed boundary layer. Considering this, parallel plate channel calculations have been performed, where the correlations consider merging of boundary layers (p. 584 – 585 in [5]). The vertical plate channels are open to the ambient air at opposite ends and are used to enhance free convection heat transfer from the base surface where the fins are attached. For symmetrically heated isothermal plates the Nusselt number is

$$\overline{\text{Nu}}_S = \frac{1}{24} \text{Ra}_S \left(\frac{S}{L} \right) \left\{ 1 - \exp \left[-\frac{35}{\text{Ra}_S(S/L)} \right] \right\}^{3/4} \quad (3.6)$$

where the average Nusselt and Rayleigh numbers are defined as

$$\overline{\text{Nu}}_S = \left(\frac{Q/A}{T_s - T_\infty} \right) \frac{S}{k} \quad (3.7)$$

and

$$\text{Ra}_S = \frac{g\beta(T_s - T_\infty)S^3}{\alpha\nu} \quad (3.8)$$

Equation 3.6 was developed for air as the working fluid, and its range of applicability is

$$\left[10^{-1} \leq \frac{S}{L}\text{Ra}_S \leq 10^5\right]$$

Optimum plate spacing is particularly important for vertical plates used as fins to enhance heat transfer by natural convection from a base surface of fixed width. If the temperature of the fins exceeds that of the ambient air buoyancy forces induce the flow between the fins. Using the foregoing correlations, fluid properties are evaluated at average temperatures of $\bar{T} = (T_s + T_\infty)/2$ for isothermal surfaces.

It should however be mentioned that for small values of H/S independent boundary layers would occur on each surface and the condition would correspond to an isolated plate [5]. Because there was not found any correlation in the literature matching the exact geometry investigated in this study the foregoing correlations were used.

3.2.3 Numerical simulations

The fin array was simulated using Comsol Multiphysics, and the results obtained in Section 3.2.1 and 3.2.2 were applied to the model. It was found that a fin spacing closer than 4.4 cm would create merging of boundary layers of each surface. From [5] correlations were used to obtain the Nusselt number for a parallel plate channel with merged boundary layers. Inserting Equation 3.7 into Equation 3.6 an expression for the heat flux is obtained

$$q = \frac{Q}{A} = \overline{\text{Nu}}_S \frac{k(T_s - T_\infty)}{S} \quad (3.9)$$

Where the heat flux was used as boundary condition for heat transfer by natural convection from the fin array to the surroundings.

Comsol Multiphysics was used to model the fin array. The heat transfer module with surface-to-surface radiation was used to find heat transfer by radiation. The surface-to-surface radiation boundary condition handles radiation with view factor calculations. The heat flux on the boundary is

$$q = \varepsilon(G - \sigma T^4) \quad (3.10)$$

where

$$G = G_m + F_{\text{amb}}\sigma T_{\infty}^4 \quad (3.11)$$

F_{amb} is the ambient view factor and G_m is the mutual irradiation coming from other boundaries in the model. Since the radiosity, J , is a function of G_m this leads to an implicit radiation balance

$$J = (1 - \varepsilon)(G_m(J) + F_{\text{amb}}\sigma T_{\infty}^4) + \varepsilon\sigma T^4 \quad (3.12)$$

The equations for surface-to-surface radiation is retrieved from Comsol's Multiphysics user's guide for the heat transfer module [2]. The reader is requested to see reference for more details.

Figure 3.3 shows the Comsol model of the fin array with boundary conditions. The blue line indicates the hot surface, while the red indicates boundaries for heat transfer by natural convection and radiation, and the dashed line represents the symmetry line. The boundary conditions set for temperatures is shown in Table 3.1 .

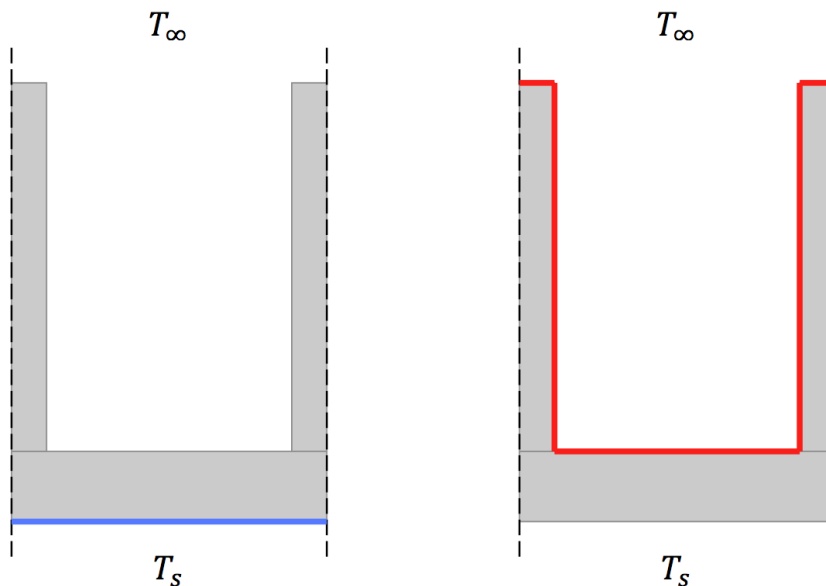


Figure 3.3: Comsol model with boundary conditions.

Table 3.1: Temperature boundary conditions for fin array in Comsol

Variable	Expression	Value	Unit
Surface temperature	T_s	393	K
Temperature of surroundings	T_{∞}	293	K

The material properties of aluminium used for the fin was built-in properties retrieved from Comsol Multiphysics, see Table 3.2, and the ambient fluid was air.

Table 3.2: Built-in material properties of aluminium from Comsol.

Variable	Expression	Value	Unit
Thermal conductivity	k	238	W/mK
Density	ρ	2700	kg/m ³
Specific heat capacity	C_p	900	J/kgK
Surface emissivity	ε	0.1	–

Since the geometry of the base surface of the fin array is set, a parametric sweep was used to identify the optimum fin height and fin spacing of the geometry. A parametric sweep takes into account a range of values for the fin height and spacing, and calculates a different results for every value.

3.2.4 Results and discussion – fin array

These results present simulations performed on the fin array. The objectives were to obtain the required rate of heat transfer, and to find the corresponding optimized heat distribution geometry. The results are based on results from the previous sections, and the fact that the boundary layers have developed on both surfaces and merged to a fully developed condition.

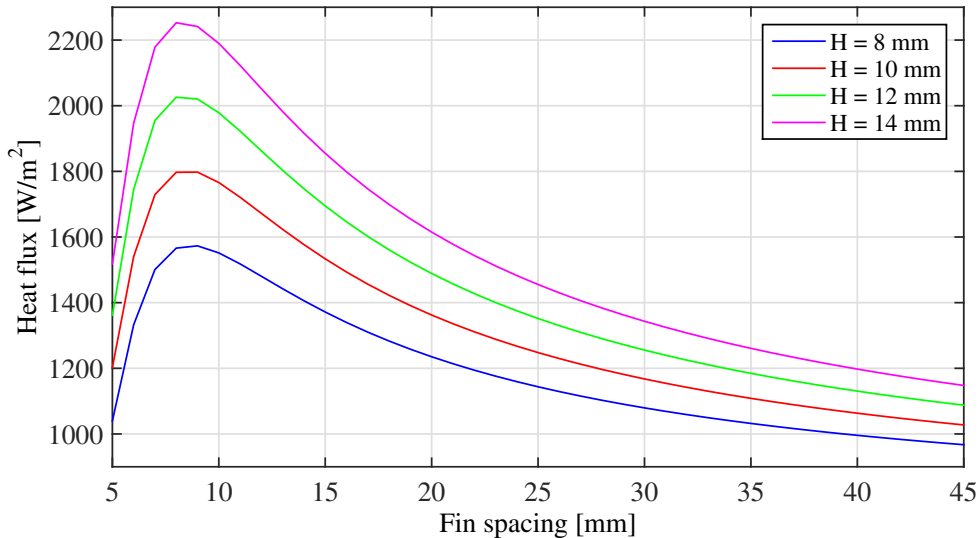


Figure 3.4: Heat flux for different fin heights with $T_s = 393$ K.

Figure 3.4 shows the heat flux for different fin heights and fin spacings. The heat flux increases until it hits a maximum and then it decreases. Regardless of increasing fin heights the optimum fin spacing is approximately 8 mm for all fin heights. The required

heat flux from the wood stove is 2200 W/m^2 , this means that the fin height must be 14 mm for a uniform base-to-ambient temperature difference of 100°C to achieve the desired effect.

When the fin spacing is decreasing, the total surface area of the fin array is increasing and thus also the heat transfer rate increases. Even though the boundary layers have already merged to yield a fully developed condition, if the fin spacing is further decreased below 8 mm it will cause resistance to the flow, and the heat transfer rate will decrease, despite the total surface area is still increasing.

In most studies fin arrays are very often considered isothermal. The temperature distribution in the fin obtained from Comsol Multiphysics shows that the temperature from the base to the tip varies by 0.2°C . Because the fin material has high thermal conductivity and the fin has a relatively short fin height and spacing the temperature does not vary significantly from the base to the tip. Assumptions of isothermal fins are therefore justified.

Comparing these results to the experiments conducted by Güvenç and Yüncü [3], and Yazicioğlu and Yüncü [14] the calculations and modeling shows good agreement with their results.

3.3 Fin channel

The fin array was closed off by adding a top plate to the fin array creating multiple channels of rectangular cross sectional area. The fin channels have a vertical base, and the fins are of constant cross sectional area. As the dimension of the base surface is set, the variables to be optimized is the fin height (H) and spacing (S). Figure 3.5 shows the geometry and dimensions of the fin channel. The study considered heat transfer from the base and fins to the air inside the channel, and heat transfer by free convection and radiation at the outer surface to the surroundings was considered. A calculation model was developed using Matlab.

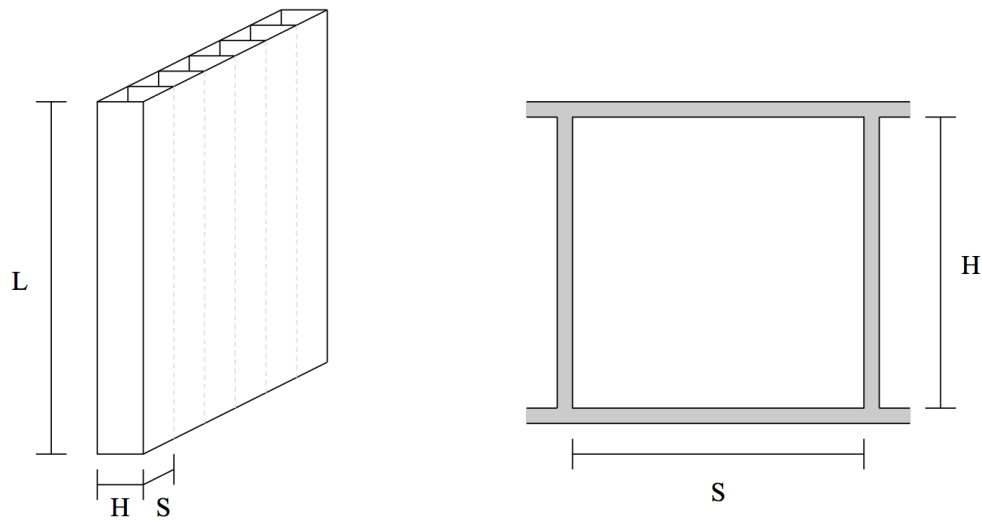


Figure 3.5: Fin channel and cross-sectional area with dimensions.

3.3.1 Mass flow for the vertical channel

Determining the heat transfer from vertical channels requires that the mass flow in the tube is known. By assuming a mass flow, the Reynolds number can be determined

$$\text{Re} = \frac{\dot{m}D_h}{\mu A_c} \quad (3.13)$$

where

\dot{m}	kg/s	mass flow
D_h	m	hydraulic diameter ($4A_c/P$)
A_c	m ²	cross-sectional area of the flow
P	m	wetted perimeter
μ	kg/sm	viscosity

Figure 3.6 shows the geometry of the channel used for heat transfer calculations. T_∞ is the inlet and surrounding temperature, T_s is the surface temperature and T_o is the outlet temperature. All surfaces are assumed to have a uniform and constant surface temperature.

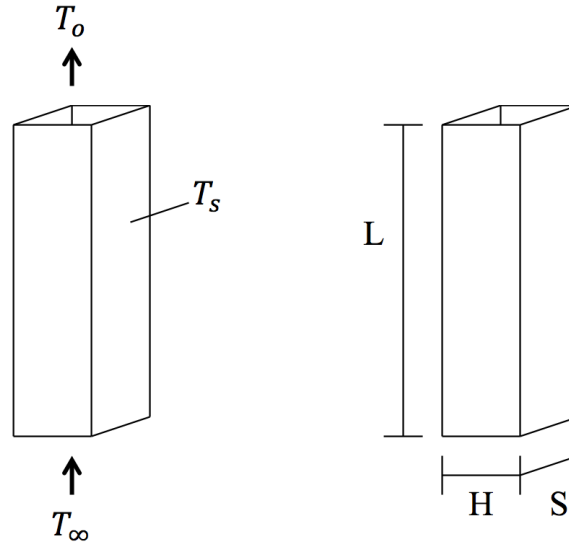


Figure 3.6: Fin channel used for calculations

If $Re \leq 2300$ the flow is laminar and the values of Table 3.3 is valid. Table 3.3 is used to calculate the heat transfer coefficient, h , and friction factor, f , for the flow in a channel of rectangular cross-sectional area. The flow is assumed to be fully developed and laminar. The entry length of the flow in the channel is not considered. This means that the Nusselt number and friction factor calculated will be smaller than if the entry length was considered.

Table 3.3: Nusselt numbers and friction factors for fully developed laminar flow in tubes of rectangular cross-sectional area (p. 519 in [5]).

$\frac{S}{H}$	$Nu_D \equiv \frac{hD_h}{k}$ (Uniform T_s)	fRe_{D_h}
1.0	2.98	57
1.43	3.08	59
2.0	3.39	62
3.0	3.96	69
4.0	4.44	73
8.0	5.60	82
∞	7.54	96

Because the ratio of S/H takes on a leap between 8 and ∞ , a curve-fit was developed. Equation 3.14 and 3.15 show the functions of the friction factor and Nusselt number as a curve-fit of Table 3.3.

$$f = \left(33.2114x^4 - 116.901x^3 + 172.997x^2 - 128.175x + 95.8858 \right) / \text{Re}_{D_h} \quad (3.14)$$

$$\begin{aligned} \text{Nu} = & -4.83846x^5 + 22.2381x^4 - 40.1790x^3 \\ & + 37.9010x^2 - 1.96819x + 7.54019 \end{aligned} \quad (3.15)$$

The heat transfer rate in the channel is calculated as follows

$$Q_1 = \dot{m}C_p\varepsilon(T_s - T_\infty) \quad (3.16)$$

where

Q_1	W	heat transfer
\dot{m}	kg/s	mass flow
C_p	J/kgK	specific heat capacity
ε	-	effectiveness
T_s	K	surface temperature of the channel
T_∞	K	temperature of surroundings

Because only the inlet temperature is known its preferable to use the NTU method. For any heat exchanger, $\varepsilon = f\left(\text{NTU}, \frac{C_{min}}{C_{max}}\right)$ (p. 689 in [5]). If the heat capacity ratio equals zero for all heat exchangers the effectiveness, ε , is

$$\varepsilon = 1 - \exp(-\text{NTU}) \quad (3.17)$$

where

$$\text{NTU} = \frac{hA}{\dot{m}C_p} \quad (3.18)$$

A is the surface area ($A = PL$) and P is the perimeter ($P = 2H + 2S$). Heat transfer in the channel can also be calculated as follows

$$Q_2 = \dot{m}C_p(T_o - T_\infty) \quad (3.19)$$

following

$$Q_1 = Q_2 \quad \Rightarrow T_o$$

$$T_o = \frac{Q_1}{\dot{m}C_p} + T_\infty \quad (3.20)$$

where T_o is the temperature at the outlet of the channel. The mean temperature in the channel can now be calculated using the log mean temperature difference

$$\Delta T_{lm} = \frac{\Delta T_2 - \Delta T_1}{\ln(\Delta T_2/\Delta T_1)} = \frac{\Delta T_1 - \Delta T_2}{\ln(\Delta T_1/\Delta T_2)} \quad (3.21)$$

$$\Delta T_{lm} = \frac{(T_s - T_\infty) - (T_s - T_o)}{\ln\left(\frac{T_s - T_\infty}{T_s - T_o}\right)} \quad (3.22)$$

The mean temperature is used to find the mean density, ρ_m , of air in the channel. Following is calculations for the pressure drop for the channel and friction, respectively

$$\Delta P_{pump} = (\rho_\infty - \rho_m)gL \quad (3.23)$$

$$\Delta P_{friction} = f \frac{L}{D_h} \frac{1}{2} \frac{\dot{m}^2}{A_c^2 \rho_m} \quad (3.24)$$

Where the pressure drop is equal ($\Delta P_{friction} = \Delta P_{pump}$), the calculations will intersect at the correct mass flow rate. Varying the geometry (height and fin spacing) of the fin channel will result in different mass flow for each geometry.

3.3.2 Heat transfer from free convection and radiation

Heat transfer from the outer surface to the surroundings is transferred by natural convection and radiation. When calculating the free convection heat transfer from a vertical plate, the Rayleigh number must first be calculated to obtain the Nusselt number (p. 571 in [5]). The Rayleigh number is

$$Ra_L = Gr_L Pr = \frac{g\beta(T_s - T_\infty)L^3}{\nu\alpha} \quad (3.25)$$

where L is the length of the base surface. For a vertical plate with natural convection the Nusselt number is

$$\overline{Nu}_L = 0.68 + \frac{0.670Ra_L^{1/4}}{[1 + (0.492/Pr)^{9/16}]^{4/9}} \quad Ra_L \leq 10^9 \quad (3.26)$$

and

$$\overline{\text{Nu}}_L = \frac{h^* L}{k} \quad (3.27)$$

For external free convection flow all thermodynamic properties of the fluid is evaluated at the film temperature $T_f \equiv (T_s + T_\infty)/2$.

Heat transfer from natural convection is then calculated as

$$Q_{conv} = h^* A (T_s - T_\infty) \quad (3.28)$$

Where $A = SL$ and h^* is the heat transfer coefficient. Radiation heat transfer from the the outer surface of the channel to the surroundings is

$$Q_{rad} = \varepsilon^* A \sigma (T_s^4 - T_{sur}^4) \quad (3.29)$$

Where $A = SL$ and ε^* is based on the material data (emissivity of aluminium). The surroundings are assumed to be at the same temperature as the ambient, $T_{sur} = T_\infty$.

3.3.3 Total heat transfer

The total heat transfer from the vertical channel to the air inside the channel is

$$Q_{ch} = \dot{m} C_p \varepsilon (T_s - T_\infty) \quad (3.30)$$

where

$$\varepsilon = 1 - \exp\left(-\frac{hPL}{\dot{m}C_p}\right) \quad (3.31)$$

Total heat transfer from the vertical channel is then

$$Q_{tot} = Q_{ch} + Q_{rad} + Q_{conv} \quad (3.32)$$

Where the total heat flux is

$$q_{tot} = \frac{Q_{tot}}{A} \quad (3.33)$$

where $A = SL$. Equation 3.32 and 3.33 shows the total heat transfer from the geometry in W and W/m^2 , respectively.

3.3.4 Fin efficiency

When calculating heat transfer for extended surfaces like fins, heat will transfer by conduction within the solid and by convection and/or radiation from the boundaries of the solid to the adjoining fluid. The theoretical fin efficiency for a straight rectangular fin of uniform cross section and an adiabatic tip is

$$\eta_f = \frac{\tanh(mL_f)}{mL_f} \quad (3.34)$$

where L_f is the length from the base to the tip of the fin. Hence, $L_f = H + S/2$, indicated in Figure 3.7 and

$$m = \left(\frac{2h}{kt} \right)^{1/2} \quad (3.35)$$

Here h is the heat transfer coefficient, t is the thickness of the fin and k is the conductivity of the fin material. The thermal conductivity of the fin material can have a strong effect on the temperature distribution along the fin and will therefore influence the heat transfer rate. The maximum heat transfer rate can be reached if the fin has no temperature gradient, this will require a large thermal conductivity and/or fin thickness.

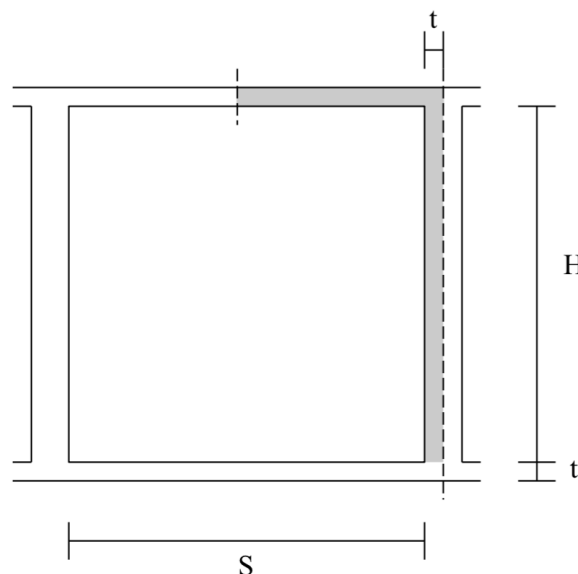


Figure 3.7: Length from base to tip of the fin.

3.3.5 Total heat transfer considering fin efficiency

This section presents the calculations of total heat transfer from the system considering the fin efficiency

$$Q_{fin \rightarrow air} = h\Delta T(A_b + A_f\eta_f) \quad (3.36)$$

Equation 3.36 determines the heat transfer from the walls of the fins to the air inside the channel. Here $A_b = SL$ is the area of the exposed base of the fin array, and $A_f = 2L_fL$ is the area of the fin.

$$Q_{fin \rightarrow \infty} = (Q_{rad} + Q_{conv})\eta_f \quad (3.37)$$

Equation 3.37 is the heat transfer from the outside of the channel to the surroundings using Equations 3.29 and 3.28 for heat transfer from radiation and free convection, respectively. The overall total heat transfer from the geometry to the surroundings (including fin efficiency) is given as

$$Q_{tot} = Q_{fin \rightarrow air} + Q_{fin \rightarrow \infty} \quad (3.38)$$

Where the total heat flux (including fin efficiency) from the geometry is

$$q_{tot} = \frac{Q_{tot}}{A} \quad (3.39)$$

Where $A = SL$.

3.3.6 Results and discussion – fin channel

These results present calculations performed on a single fin channel. The objectives were to ensure that the heat transferred from the heat storage to the surroundings fulfill the required rate of heat transfer, and to find a corresponding optimized heat distribution geometry. The results are based on results from the previous sections, and the fin efficiency is considered in all results.

Figure 3.8 shows the heat flux for different fin heights with a constant surface temperature of 393 K. The figure shows the heat flux for the length of the fin geometry. A closer fin spacing will lead to an increased heat transfer area and numerous fins, while a large fin spacing will lead to fewer fins and a smaller heat transfer area.

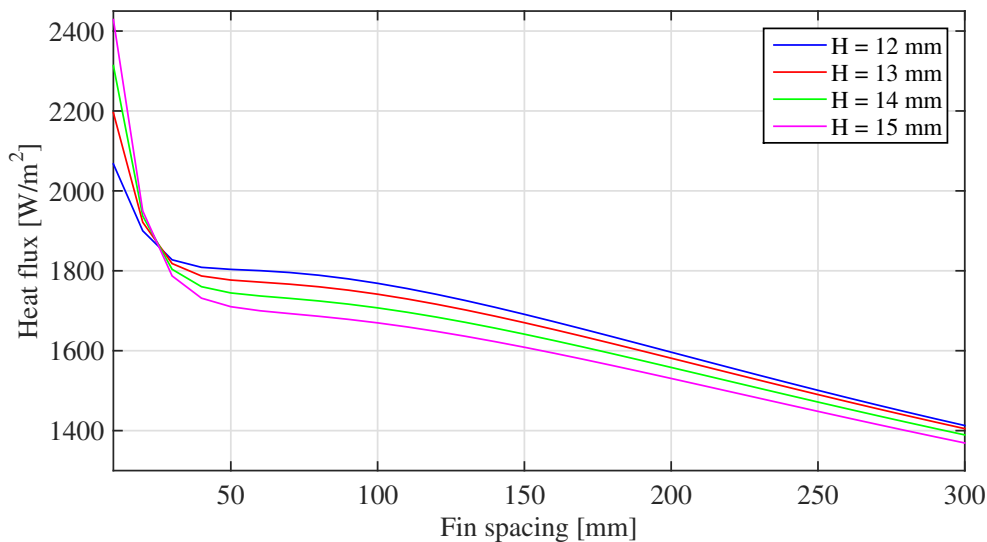


Figure 3.8: Heat flux for $H = 15$ mm for different surface temperatures.

Figure 3.9 shows the same as Figure 3.8 only with a closer view. The figure shows that a fin height of 14 mm or 15 mm, and a base-to-ambient temperature difference of 100°C meets the requirements of a heat transfer rate of 2200 W/m^2 . Based on these results it was decided to proceed with a fin geometry with a fin height of 15 mm and a fin spacing of 14 mm.

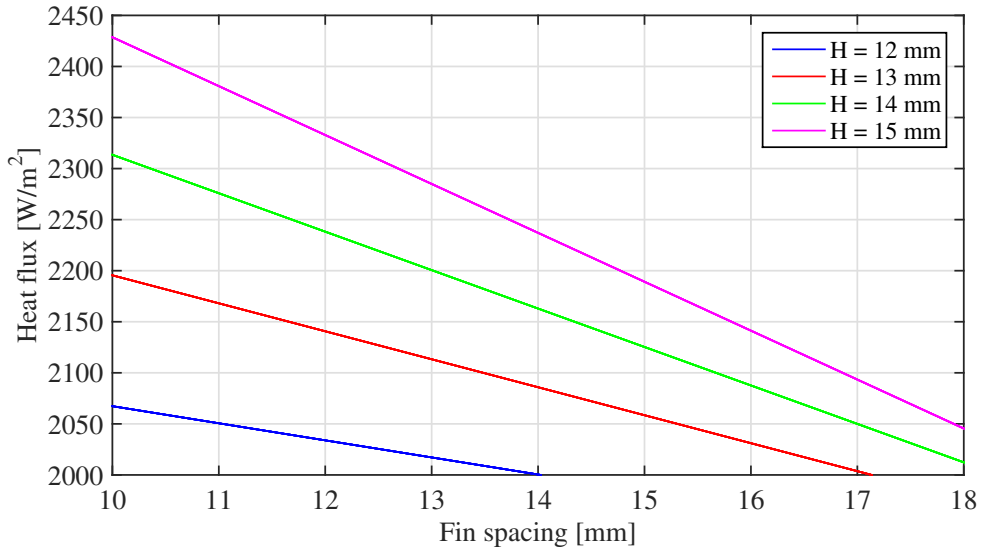


Figure 3.9: Heat flux for $H = 15$ mm for different surface temperatures.

Figure 3.10 shows the fin efficiency for a fin height of 15 mm. It is preferable to have a high fin efficiency and it is seen that for smaller spaced channels the fin efficiency is higher. For the fin geometry of choice the fin efficiency is 99%, which is very satisfactory.

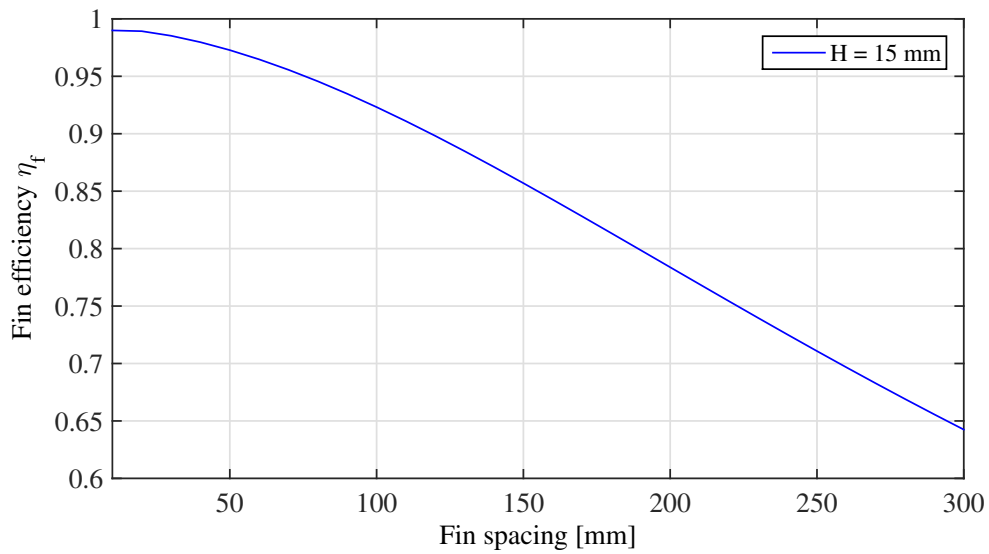


Figure 3.10: Fin efficiency for a fin height of $H = 15$ mm with $T_s = 393$ K.

CHAPTER 3. HEAT REJECTION MODEL

Before firing up a wood stove the temperature inside the stove will be equal to the surrounding air. When firing up in the wood stove the temperature will increase and reach its maximum, before it decreases and yet again will reach the surrounding temperature. Figure 3.11 shows the heat flux for a fin height of $H = 15$ mm for different surface temperatures. The figure shows how much heat flux is expected to be attained from different surface temperatures in the stove. If the surrounding temperature is 20°C and equal to the temperature in the wood stove the heat flux will be zero.

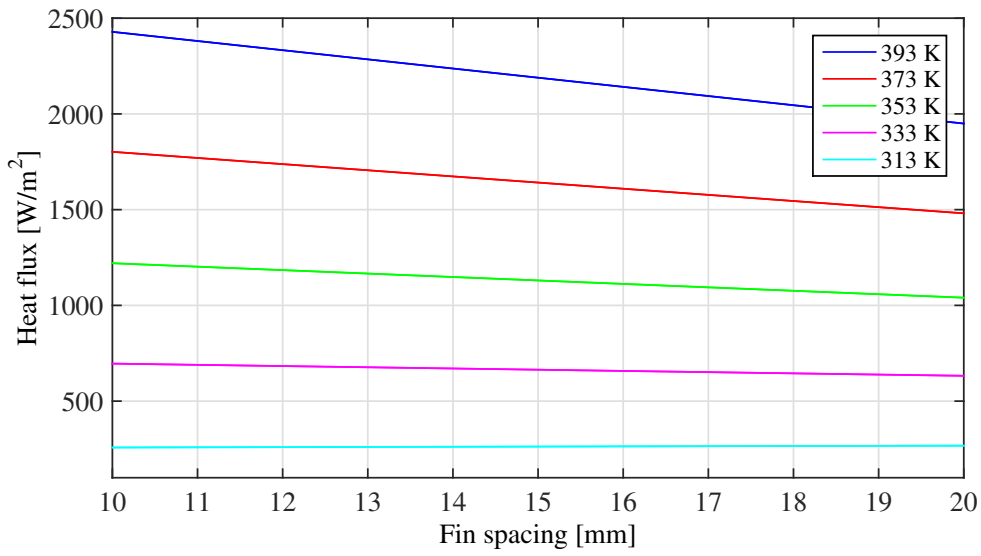


Figure 3.11: Heat flux for $H = 15$ mm for different surface temperatures.

3.4 Summary, conclusions and discussion

For the fin array It was found that the boundary layers forming on each plate was merged to yield a fully developed condition if the fins were spaced closer than 4.4 cm. The optimum fin spacing was found to be approximately 8 mm independent of the size of fin heights. This showed that the fin spacing was a constant factor of approximately 8 mm for the optimum fin geometry. To meet the requirements of heat transfer from the wood stove to the surroundings of 2200 W/m^2 , the optimum fin geometry was found to be a fin height of 14 mm or 15 mm with a fin spacing of 8 mm, for a base-to-ambient temperature difference of 100°C .

A top plate was added to the fin array, creating multiple fin channels. The optimum fin geometry for the channel was found to be a fin height of 15 mm with a fin spacing of 14 mm, for a base-to-ambient temperature difference of 100°C . It was shown that for different surface temperatures of the fin channel the heat flux will decrease rapidly for low surface temperatures. A significant decrease in heat flux of approximately 30% was found for a decrease in temperature of 20°C from 120°C to 100°C .

Both fin arrangements achieved the required rate of heat transfer from the fin arrangement to the surroundings. It was however decided to proceed with the fin channel arrangement. The main reason for this choice was that this wood stove is to be adapted to houses and having fin arrays with hard edges can be impractical, the fin channel arrangement is a more esthetic choice. The fin spacing of the channel is also larger than for the array, meaning that fewer channels are needed.

Chapter 4

Heat storage study

4.1 Introduction

Experimental studies were performed on a PCM heat storage unit. The experiments were initially intended to be performed using a PCM as well as a PCM containing metal fins or foam to enhance the heat transfer rate. Unfortunately the test rig was not built in time to perform experiments on the storage unit containing fins or foam. The objectives of the experiments were to determine the effective thermal conductivity and the net energy storage capacity. Due to the fact that the experiments were performed using PCM only, the objective was changed and the effective thermal conductivity of PCM was determined instead. The temperature response, heat distribution, and the effect of natural convection on the melting of the PCM were also studied.

Two different experimental setups were studied. In the first case the top surface of the heat storage unit was heated, in the second case the heat storage unit was turned upside down and heated from below. The experimental setup and test rig was otherwise identical for both experiments. Results from experiments were compared with results from numerical simulations. An uncertainty analysis was performed on the thermal conductivity obtained from the experiments. The uncertainty analysis is documented in Appendix C, but highlights are presented in Section 4.7.

The phase change material used in these experiments was erythritol. Erythritol is a sugar substitute and has suitable properties as a PCM. The material properties of erythritol is presented in Appendix, Table A.3.

4.2 Test rig

Figure 4.1 shows the experimental setup of the test rig. The heat storage unit (3) consists of an outer shell made of teflon filled with PCM. A solid aluminium block is placed at the top and bottom (1,5). The heat storage unit is heated with a cartridge-type heater (6) placed inside the center of the aluminium block, at the top of the heat storage. Nine thermocouples (4) are placed inside the heat storage unit where they measure the temperature in the axial direction. Five is placed on one side, and the other four on the other side.

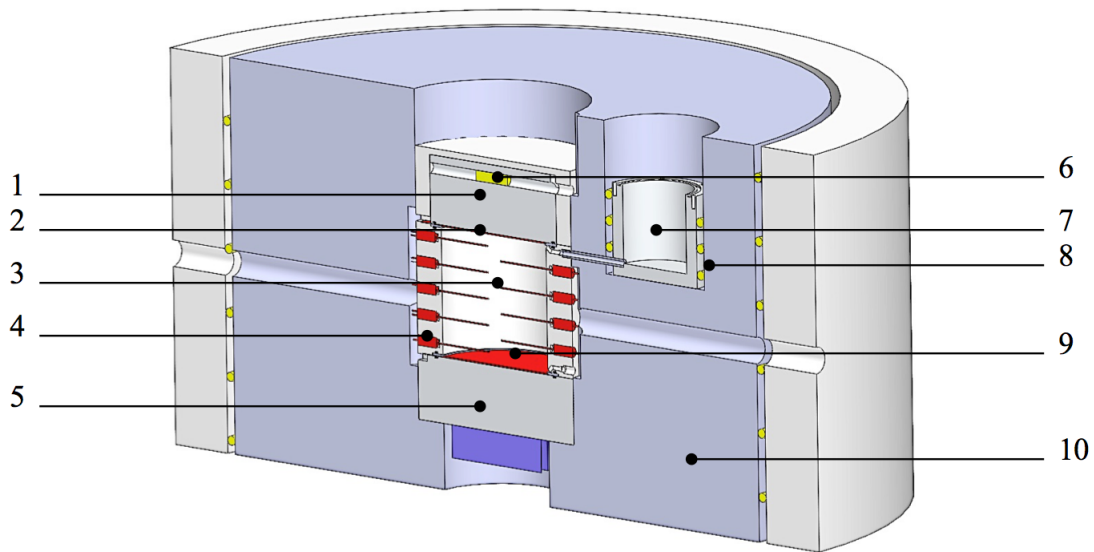


Figure 4.1: Experimental setup.

1	Aluminium block	6	Cartridge heater
2	Heat flux sensor	7	Expansion chamber
3	Heat storage unit	8	Wire heater
4	Thermocouple	9	Flux sensor
5	Aluminium block	10	Insulation

When erythritol is melting, its volume will expand with approximately 10% [7]. The expansion chamber (7), located to the right, has a small passage to the heat storage where the expanded erythritol can escape. The expansion chamber is heated from the outside (8) to prevent solidification and clogging of PCM. Two flux sensors are placed inside the storage unit, one at the top surface and one at the bottom (2,9). It is important that the heat storage unit is completely filled with PCM before starting an experiment, so that it has close thermal contact with the heat flux sensors and heat source. The test rig is insulated (10) using silcapor and rockwool. The dimensions of the heat storage unit is $D = 100$ mm and $L = 100$ mm.

Figure 4.2 is a sketch showing the positions of the temperature indicators. TT01 to TT09 is the thermocouples located inside the heat storage unit. Thermocouple TT01 and TT05 are placed 10 mm from the top and bottom, respectively. The remaining thermocouples are placed 10 mm apart in the axial direction, and about 5 mm from the center in the radial direction. TT10 is the temperature sensor measuring the temperature outside the expansion chamber. TT11 is the temperature sensor measuring the temperature of the passage between the heat storage unit and the expansion chamber. TT12 is the temperature sensor that measures the temperature at the bottom outside the heat storage unit and TT13 is the temperature sensor measuring the temperature of the cartridge heater.

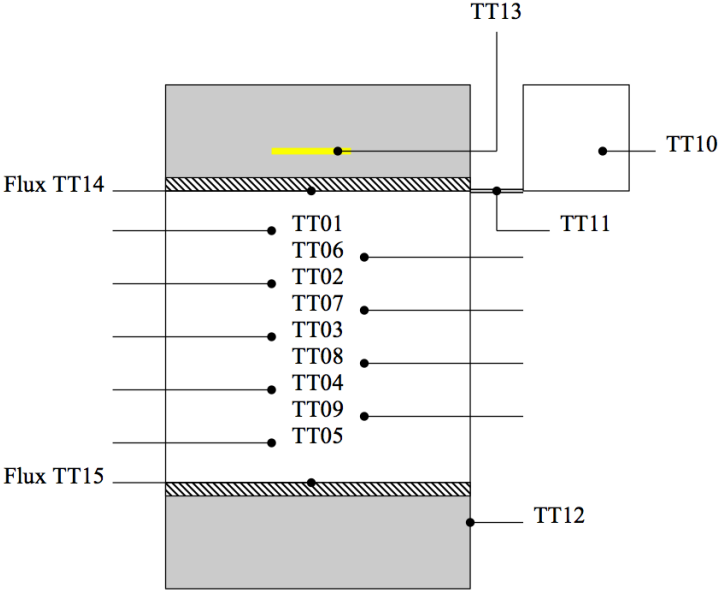


Figure 4.2: Positioning of thermocouples TT01 to TT09 inside the heat storage.

TT01 – TT09	Thermocouple	TT13	Cartridge heater
TT10	Expansion chamber	TT14	Heat flux sensor
TT11	Passage	TT15	Heat flux sensor
TT12	Outer surface of heat storage unit		

When the experiment starts the heat storage unit is completely filled with solid PCM and the outside of the storage unit is insulated. The wire heating at the outside of the expansion chamber is the first to be enabled, this is to melt the leftover PCM in the expansion chamber to prevent clogging in the small passage between the heat storage unit and the expansion chamber when the PCM inside the storage is melting. The cartridge heater located inside the aluminium block is set to 150°C, and temperatures TT10 and TT11 are kept at 5°C – 10°C above temperature TT13. Keeping temperatures TT01 and TT11 just above TT13, will prevent the excessive heat from the side from being too high. Labview was used to log the different temperatures and heat fluxes inside the storage unit during the experiments.

4.3 Heat storage unit heated from the top

The heat storage unit was filled with PCM and heated from the top surface. The experimental setup was described in Section 4.2. Figure 4.3 shows a simplified model of the experimental setup. The yellow indicates the cartridge heater and red the melting front.

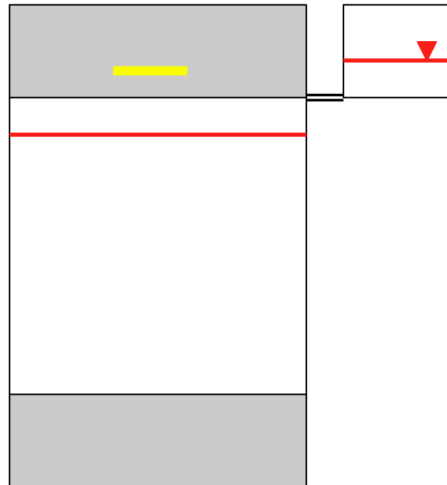


Figure 4.3: PCM heat storage unit heated from the top.

Figure 4.2 shows the positioning of thermocouple TT01 to TT09 inside the storage unit. Preparing an experiment includes arrangement of the thermocouples inside the storage unit. Table 4.1 shows their actual position, defining the length of the storage as L , and the top as $L = 0$ mm. The table shows that the distance between the positioning of the thermocouples vary between 8 mm – 12 mm, when the initial difference in their positions should be 10 mm. This is because the thermocouples have no support inside the storage unit and they are quite thin, therefore they bend easily. The experiment was run for 25 hours.

Table 4.1: Actual position of thermocouples inside the heat storage unit.

Thermocouple	Position [mm]	Thermocouple	Position [mm]
TT01	9	TT06	17
TT02	28	TT07	39
TT03	50	TT08	59
TT04	71	TT09	79
TT05	90		

4.3.1 Numerical model - heat storage unit heated from the top

Figure 4.4 shows the setup of the PCM heat storage unit heated from the top surface. The figure shows a 2D axisymmetric model. The storage unit is made of teflon and insulated using silcapor. The black dots located to the left and close to the symmetry line are the positions of the thermocouples, positioned according to Table 4.1.

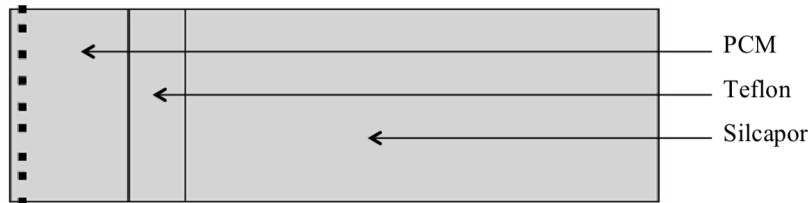


Figure 4.4: Setup of PCM heat storage unit heated from the top modeled using Comsol.

The numerical simulation is a simplified version of the experiments. Figure 4.5 shows the boundary conditions used for the numerical simulations. The blue line indicates where the model is insulated. Temperature for TT01 and TT05 obtained from the experiment is used as boundary condition for hot and cold surface, respectively. From the storage to the surroundings a heat transfer coefficient of magnitude $5 \text{ W/m}^2\text{K}$ is used. This represents the heat transfer from the insulated storage to the surroundings.

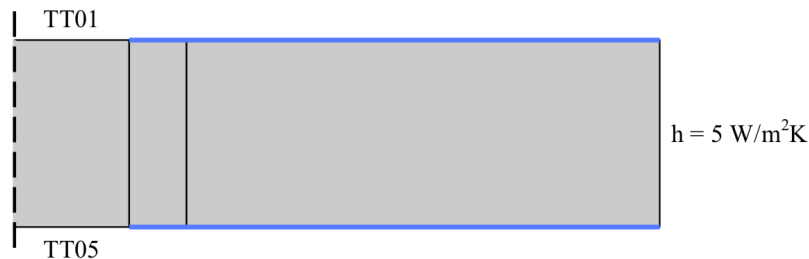


Figure 4.5: PCM heat storage unit heated from the top, with boundary conditions shown.

The thermal conductivity of liquid erythritol was obtained from the experiment and is presented in Section 4.6. The other material properties of erythritol was obtained from the experiment by co-supervisor and PhD candidate, Krisjansson. Table 4.2 shows the values used, where ρ and C_p are functions of temperature. When the temperature increases the material properties of erythritol change. Table 4.2 shows the mean value for ρ and C_p for the solid and liquid phases.

Table 4.2: Material properties of erythritol employed in Comsol.

Variable	Expression	Value	Unit
Thermal conductivity, solid	k_s	0.78	W/mK
Thermal conductivity, liquid	k_l	0.40	W/mK
Density	ρ	$\rho(T)$	kg/m ³
Specific heat capacity	C_p	$C_p(T)$	J/kgK

4.4 Heat storage unit heated from below

Figure 4.6 shows the experimental set up of the PCM heat storage unit heated from below. To prevent liquid PCM from running out of the expansion chamber compressed air was used to keep the pressure in equilibrium using the principles of Equation 4.1. The flow of compressed air was controlled by a valve and the water in the tank ensured that the pressure of the air was kept in equilibrium with the hydrostatic pressure. The experiment was otherwise identical to the experiment where the heat storage unit were heated from the top.

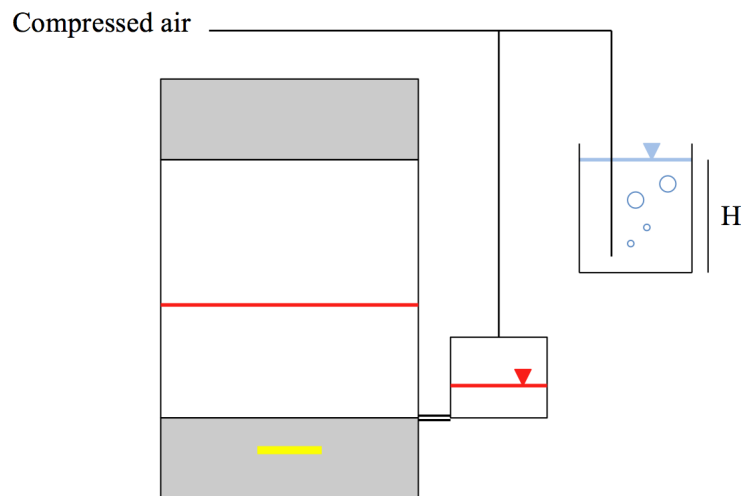


Figure 4.6: PCM heat storage unit heated from below with compressed air system.

$$\Delta p_{\min} = \rho_{\text{water}} g H_{\text{water}} > \rho_{\text{PCM}} g H_{\max, \text{PCM}} \quad (4.1)$$

4.4.1 Numerical model – heat storage unit heated from below

A 1D model was developed for the heat storage unit heated from below. Figure 4.7 shows a sketch of the model. The challenge was to develop a numerical model considering a moving boundary with free convection heat transfer in the liquid phase. The heat fluxes

obtained from the experiment (TT14 and TT15) were calibrated and used as boundary conditions for the comparison. The boundary condition is applied to point 1 and 3 in the sketch. The first domain (1-2) is set to have liquid properties, and the second domain (2-3) to have solid properties.

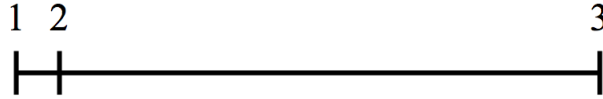


Figure 4.7: Sketch of Comsol model for experiment heated from below.

Point 2 in the sketch presents the moving melting front. When the temperature of the PCM has reached the melting temperature point 2 will start to move to the right, symbolizing the melting front. The velocity of the melting front is calculated as follows

$$v = \frac{-(\text{up}(q) - \text{down}(q))}{\rho_s H_{sl}} \quad (4.2)$$

where

$$\text{up}(q) = \left(\frac{dT}{dx} k \right)_{\text{solid}, x=S} \quad \text{down}(q) = \left(\frac{dT}{dx} k \right)_{\text{liquid}, x=S} \quad (4.3)$$

and S is the position of the melting front.

Table 4.3 shows the material properties used for the comparison. $k(S)$ is the effective thermal conductivity for the liquid phase obtained from the experiment and presented in Section 4.6. $k(S)$ is a function of the melting front position. It is assumed that the effective conductivity of liquid erythritol obtained from a horizontal melting front is similar to a vertical melting front. The other material properties are obtained from the experiment by Krisjansson (see Table 4.2) and the mean values for these are presented in Table 4.3.

Table 4.3: Material properties of erythritol employed in Comsol.

Variable	Expression	Value	Unit
Thermal conductivity, solid	k_s	0.78	W/mK
Thermal conductivity, liquid	k_l	$k(S)$	W/mK
Latent heat	H_{sl}	336	kJ/kg
Density, solid	ρ_s	1480	kg/m ³
Density, liquid	ρ_l	1278	kg/m ³
Specific heat capacity, solid	C_{p_s}	1690	J/kgK
Specific heat capacity, liquid	C_{p_l}	3160	J/kgK

4.5 Results and discussion

4.5.1 Heat storage unit heated from the top

Figure 4.8 shows the measured temperatures for each of the thermocouples obtained from the experiment where the heat storage unit was heated from the top. It takes about 5 hours for the first thermocouple, TT01, to reach the melting temperature of 118°C . Based on the positions of the thermocouples, at this point about 9% (or 9 mm) of the PCM had melted. At the end of the experiment, after 25 hours, only three more thermocouples have reached the melting temperature. Assuming a uniform melting front, only 30% (or 30 mm) of the PCM had melted at this point.

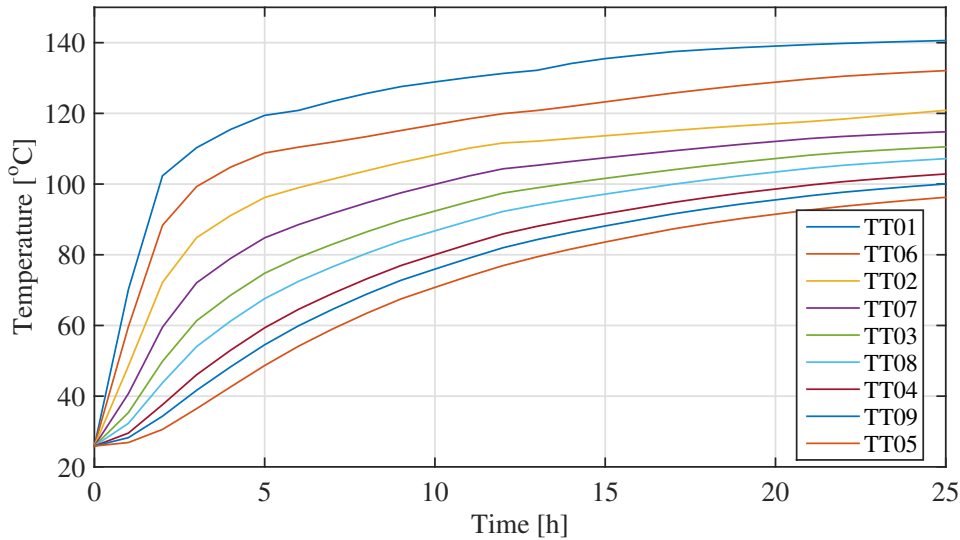


Figure 4.8: Measured temperatures in the storage unit for thermocouples TT01 to TT09.

Figure 4.9 shows the temperature for each of the thermocouples from numerical simulations compared to the results from the experiment. The blue line indicates data from the experiment and the red line indicates data from Comsol Multiphysics. The position of the thermocouples TT01 to TT09 are identical to Figure 4.8. Because the temperatures obtained from the experiment for thermocouple TT01 and TT05 is used as boundary condition, the comparison of data for temperature TT01 and TT05 from numerical simulations compared to data from the experiment are identical.

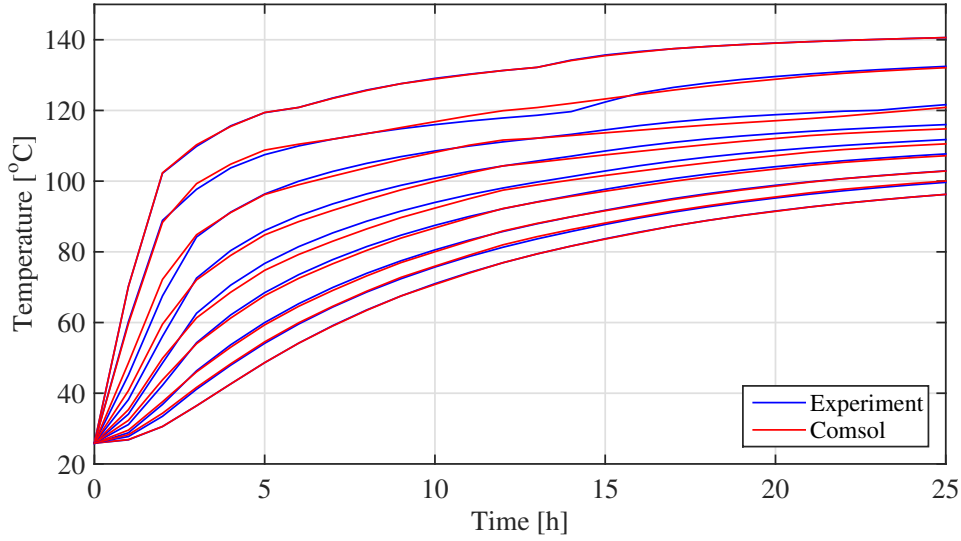


Figure 4.9: Temperature of each thermocouple from Cmsol compared to experiment

The comparison shows excellent agreement, where the average relative error is calculated to be 0.8%. A possible source of error is the positioning of the thermocouples. Because the thermocouples have no support, there is no way to control their actual position. When the erythritol is solidified the material tends to crystallize into everything from small to large crystals. This could cause the thermocouples to bend their positions, as they are quite thin and bend easily.

One of the objectives of the experiment was to determine the net energy storage capacity in the storage unit. A simple numerical model was used to calculate the total internal energy in the heat storage unit. Calculations are documented in Appendix B. Table 4.4 shows the total net heat storage capacity at steady state, and the amount of latent and sensible heat. The total net energy is 336.8 kJ, where 43% of the heat is stored as latent heat in liquid phase. The difference in the total heat from calculations compared to Cmsol Multiphysics is 4%.

Table 4.4: Net heat storage capacity found using Cmsol

Variable	Expression	Value	Unit
Total internal energy	E_{tot}	336.8	kJ
Latent heat	E_{latent}	148.7	kJ
Sensible heat	E_{sensible}	200.4	kJ

4.5.2 Heat storage unit heated from below

Figure 4.10 shows the comparison of the melting front from the experiments and the model used in Comsol Multiphysics. The obtained melting front position from the experiment was calculated based on the measured temperatures and positioning of the thermocouples. The figure shows that during the experiment all the PCM in the heat storage is melted after 65,000 s (18 hours). The results from the simulation show that the PCM starts to melt at a later point in time, and that all the PCM is melted after 72,000 s (20 hours).

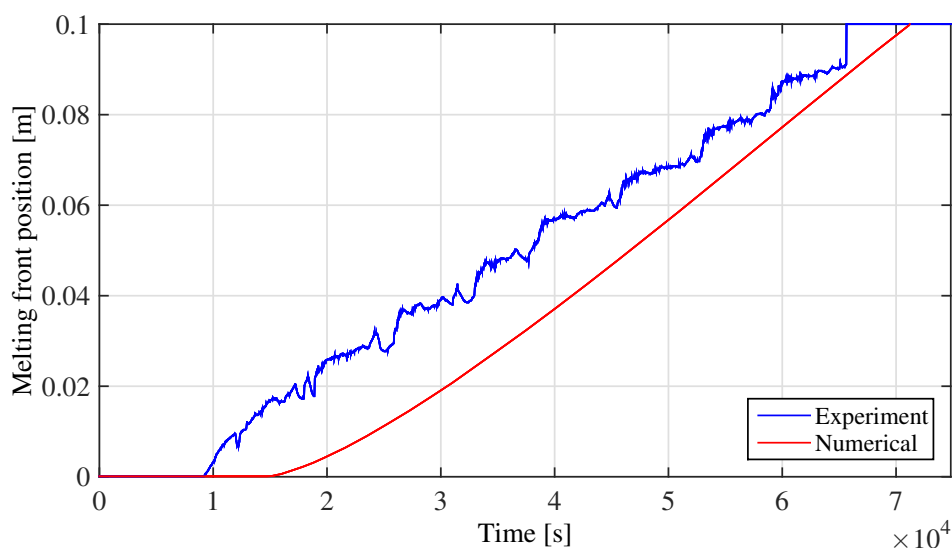


Figure 4.10: Comparison of melting front for experiments and numerical model

There are particularly two things to point out when it comes to the comparison. First, the numerical model starts to melt after about 15,000 s, this is 5,000 s longer than during the experiment. This shows a significant difference in the starting time of the melting. The reason why is because the thermal conductivity used in the simulations is estimated too high. When the conductivity is estimated to high the heat is used to increase the temperature of the solid PCM instead of melting the PCM. Secondly, the gradient of the curve from simulation does not match the gradient of the curve from the experiment. This can be explained by looking at the boundary condition used on the cold surface of the model. Instead of forcing a boundary condition, a thermal mass (the aluminium heat spreader) could be included in the model to better simulate the experiments. This would give more realistic temperature profiles.

After the second experiment was conducted it was discovered that the heat flux measurements were affected by the melting/solidifying of the PCM. The PCM had leaked into the heat flux sensor contributing to increasing the resistance in the sensor, causing the results based on the heat flux measurements to be unreliable.

4.6 Thermal conductivity

PCMs used for heat storage have poor thermal conductivity. Enhancing the conductivity by adding metal foam/fins will accelerate the phase change process without significantly reducing the PCMs heat storage capacity. The objectives of the experiments were to measure the effective thermal conductivity of erythritol containing metal foam/fins. Since the test rig was not built in time to perform experiments on the effective thermal conductivity of erythritol, the objective was changed and the thermal conductivity of erythritol was determined instead. Material property data was compared to literature data. Literature values of erythritol is presented in Appendix, Table A.3.

The properties were obtained using data processing with Matlab and numerical simulation using Comsol Multiphysics. Kristjansson, developed the Matlab computer code and model in Comsol Multiphysics used in the calculations. Kristjansson also performed the measurement of conductivity for solid erythritol. The conductivity of the solid phase was obtained using a Hot Disk instrument for thermal conductivity measurement. The result is presented in Table 4.5, and shows a significant increase of 7% compared to literature values.

Table 4.5: Thermal conductivity of solid erythritol determined using Hot Disk

Variable	Expression	Value
Thermal conductivity, solid	k_s	0.78 W/mK
Thermal conductivity, solid (literature value)	k_s	0.73 W/mK

Thermal conductivity for liquid phase of PCM was determined from the experiment where the heat storage unit was heated from the top. The conductivity was found by comparing data from the experiment with data obtained from numerical simulations. The conductivity for solid erythritol obtained by Kristjansson was used in the calculations. A range of conductivities for liquid phase from 0.2 – 0.6 W/mK was tested. Figure 4.11 shows the conductivity of liquid erythritol to average relative error. The figure shows the average relative error for every conductivity of liquid PCM from 0.2 – 0.6 W/mK. Where the graph reaches its minimum, is the value for conductivity of liquid phase with the smallest average relative error. Table 4.6 shows the obtained value. A comparison of the obtained conductivity to literature value show a significant increase of 21%.

Table 4.6: Thermal conductivity of liquid erythritol found from experiment with storage unit heated from the top.

Variable	Expression	Value
Thermal conductivity, liquid	k_l	0.40 W/mK
Thermal conductivity, liquid (literature value)	k_l	0.33 W/mK

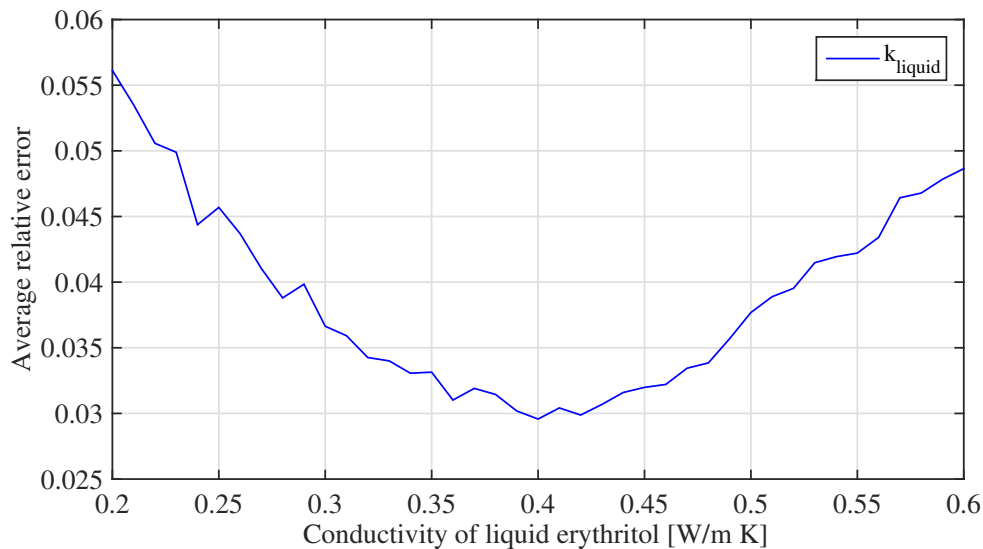


Figure 4.11: Thermal conductivity of liquid erythritol to average relative error.

A heat storage unit heated from below must consider heat transfer by natural convection in the liquid phase. When PCM is melting the effective thermal conductivity will increase as the melting front progresses. Figure 4.12 shows the effective thermal conductivity of liquid erythritol obtained from the experiment where the heat storage unit was heated from below. Calculations were performed using the basic equation of Fourier’s law for heat conduction

$$k_l = \frac{qL}{(T_h - T_m)} \tag{4.4}$$

where

- k_l W/mK liquid conductivity
- q W/m² heat flux
- L m length of melting front
- T_h K hot temperature
- T_m K melting temperature

Because the calculation of the effective thermal conductivity of erythritol was based on heat flux measurements, it was for this case assumed that the heat flux sensors were working properly.

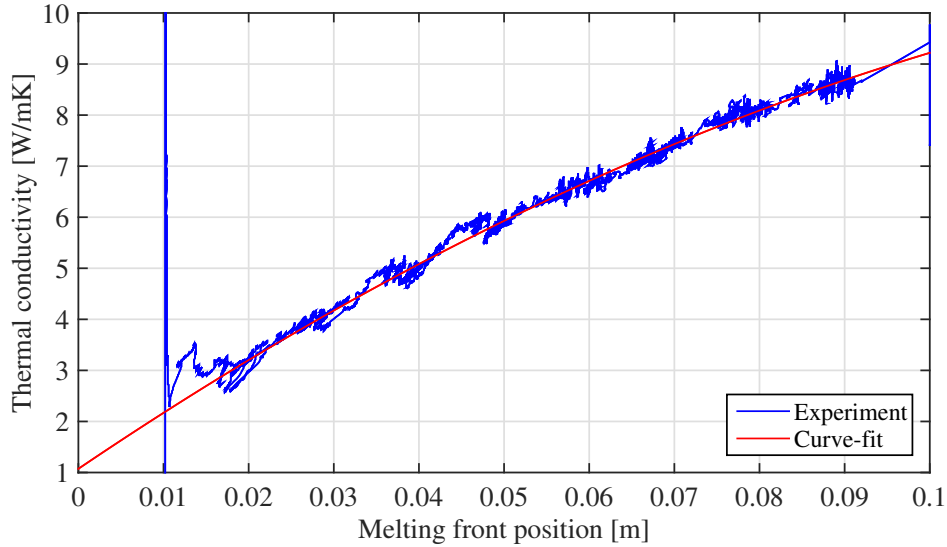


Figure 4.12: Effective thermal conductivity of liquid erythritol from experiment with curve-fit.

The position of the melting front was calculated based on temperature measurements and positioning of the thermocouples. The calculation of the effective thermal conductivity is therefore uncertain in the interval between TT01 and TT05 (i.e. 0 – 0.01 m). Because the effective thermal conductivity obtained from the experiment was irregular, a curve-fit was adapted to the graph from 0.018 m – 0.09 m, with linear extrapolation. Equation 4.5 shows the curve-fit formula used for the calculations. The curve-fit shows that the effective conductivity ranges from 1.18 – 9.25 W/mK.

$$y = -312.54x^2 + 112.72x + 1.0727 \quad (4.5)$$

4.7 Uncertainty analysis

An uncertainty analysis was performed for the measured thermal conductivities of erythritol. The highlights of the analysis is presented in this section, where the full analysis can be viewed in Appendix C. The procedure of the analysis is performed according to Moffat [9] and Wheeler and Ganji [13]. Thermal conductivity of erythritol was measured and determined for both the solid and the liquid phase. Thermal conductivity for the solid phase was determined using a Hot Disk instrument, where Kristjansson performed

the measurements. The two conductivities of liquid erythritol were obtained from each of the experiments described above.

The conductivity of solid erythritol was measured to be 0.78 W/mK, where the Hot Disk instrument has an uncertainty of $\pm 5\%$. Table 4.7 shows the nominal value obtained for conductivity of solid erythritol and its uncertainty.

Table 4.7: Uncertainty of conductivity of solid erythritol obtained using Hot Disk.

Variable	Value (W/mK)	Uncertainty
k_{solid}	0.78	$\pm 5.0\%$

Thermal conductivity of liquid erythritol from experiment where the heat storage unit was heated from the top was found by doing data-processing and comparing the experimental data to data from a numerical model. Table 4.8 shows the nominal value and uncertainty of the liquid conductivity of erythritol based on the experiment when the heat storage unit was heated from the top.

Table 4.8: Uncertainty of conductivity of liquid erythritol obtained from experiment with storage unit heated from the top.

Variable	Value (W/mK)	Uncertainty
k_{liquid}	0.40	$\pm 31.2\%$

The effective thermal conductivity of liquid erythritol from experiment heated from below was found by doing data-processing and using Equation 4.4. Table 4.9 shows the average uncertainty of liquid erythritol obtained from the experiment where the heat storage unit was heated from below. As the nominal value of the effective thermal conductivity is changing with time the *average* uncertainty was calculated by considering three different time steps, 20,000 s, 40,000 s and 60,000 s, respectively.

Table 4.9: Average uncertainty of effective thermal conductivity of liquid erythritol obtained from experiment with storage unit heated from below.

Variable	Value (W/mK)	Uncertainty
k_{liquid}	k(S)	$\pm 6.9\%$

4.8 Summary, conclusions and discussion

Two different experiments were conducted on a PCM heat storage unit where both experiments had identical experimental setup. In the first experiment the storage unit was heated from the top surface. From the results it was found that 30% of the PCM inside the heat storage unit had melted after 25 hours. The results were compared to results from numerical simulations where the agreement was very good and a relative average error was calculated to be 0.8%

In the second case the heat storage unit was turned upside down and heated from below. After 18 hours all of the PCM in the storage unit had melted. This proves that free convection heat transfer has a significant impact on the melting pace of the PCM. The results from the experiments were compared to results from numerical simulations. The comparison of the melting front did not show an immediate agreement or similar behaviour. After the second experiment was conducted it was discovered that the heat flux measurements were affected by the melting/solidification of the PCM. The results based on the heat flux measurements are therefore unreliable.

For the PCM heat storage unit heated from the top the net energy storage capacity was 336.8 kJ at steady state, where 43% of the heat was stored as latent heat. Unfortunately it was not possible to determine the net energy storage capacity for the storage unit heated from below due to the fact that heat provided until steady state was not reachable.

A total of three conductivities of erythritol were obtained. Conductivity of solid erythritol was obtained by Kristjansson using a Hot Disk instrument, while the conductivity of the liquid phase was found one from each experiment. An uncertainty analysis was performed on the measured conductivities. The conductivity for solid phase showed the lowest uncertainty of $\pm 5\%$, while the thermal conductivity obtained from the experiment heated from the top show an uncertainty of $\pm 31\%$. The results showed that the method employed for studying the effective conductivity was inaccurate.

Chapter 5

Overall PCM heat storage model

5.1 Heat supply, storage and distribution

An overall heat storage model was developed in order to simulate heat supply, storage and distribution to the surroundings. The study included the use of a PCM and the same PCM with aluminium foam with a porosity of 95%. Adding aluminium to the PCM enhances the heat distribution in the heat storage unit and also the heat transfer rate to the surroundings.

A heat flux based on calculations of batch combustion of wood was supplied to the PCM heat storage unit. The benefit of using a PCM heat storage unit in combination with a wood stove is that the heat supply from the wood stove should be absorbed by the storage unit and stored as latent heat. The temperature response of the PCM storage unit should be fast, and the rate of heat rejected to the surroundings should be increased and even.

Results obtained previously in this study were used in the simulations. In Chapter 3 an optimum fin geometry for heat rejection to the surroundings was found. This geometry was applied to the heat storage unit at cold surface (see Figure 5.2). In Chapter 4 the effective thermal conductivity of erythritol was found. The effective conductivity was used in material data for erythritol in the model.

The overall heat storage model has two main requirements that it must fulfill. The temperatures in the heat storage unit should not exceed 150°C to keep the PCM from degrading, and the required heat transfer rate from the heat storage unit to the surroundings should be at least 2200 W/m².

Further objectives of this study were to investigate the effect aluminium foam has on the heat transfer and internal temperature distribution.

Figure 5.1 shows a sketch of the heat flux from the wood stove supplied to the PCM heat storage unit which is mounted with a fin arrangement. For an actual wood stove three of the vertical surfaces would be mounted with a PCM heat storage unit and fin arrangement.

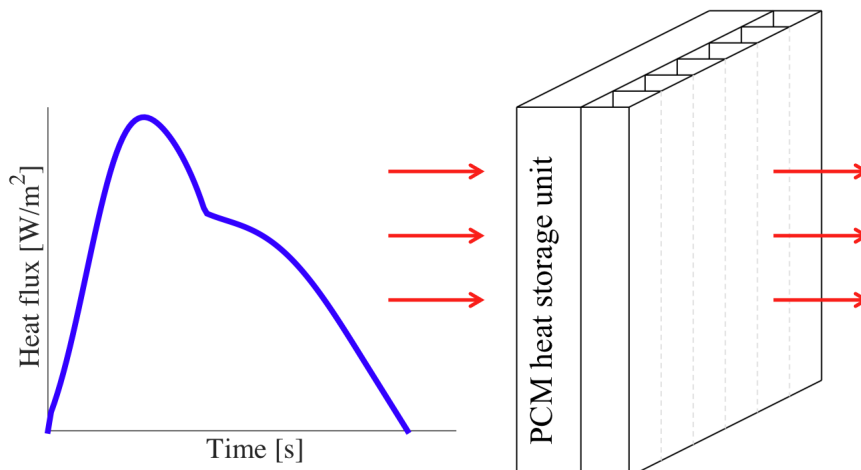


Figure 5.1: Sketch of a PCM heat storage unit mounted with a fin arrangement.

5.2 Numerical model and boundary conditions

Figure 5.2 shows a simple model of the heat storage unit indicated with hot and cold surfaces. The model had the same setup as the experiment where the heat storage unit was heated from below. The model is described in Section 4.4.1 and Figure 4.7 shows a sketch of the model.

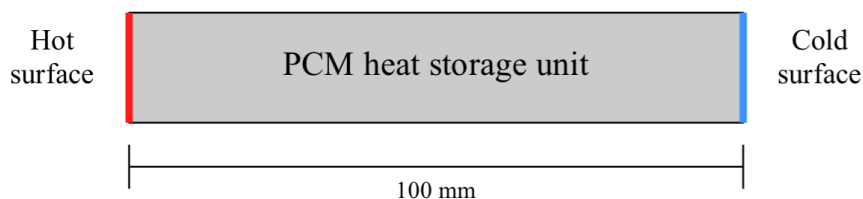


Figure 5.2: PCM heat storage unit with hot and cold surfaces.

The heat storage unit was supplied with a heat flux at hot surface that was based on calculations of batch combustion of wood. Figure 5.3 shows the combustion for one batch of wood. Data for the wood combustion were received from Kristjansson. When the heat flux is increasing the temperature at hot surface will increase. When the hot surface reach the melting temperature of 118°C the PCM inside the heat storage unit will start to melt and the moving boundary of the model will start to move according to the melting front.

When the heat flux is decreasing the temperature at hot surface will decrease, and the PCM inside the storage unit will start to solidify. At this point the moving boundary started moving back to the starting point.

The difference between the overall heat storage model and the model used for comparison with the experiment where the heat storage unit was heated from below, was that the experiment considered only melting. When solidifying of the PCM not considered the moving boundary will not have to move back to the starting point because all of the PCM in the heat storage unit will have melted.

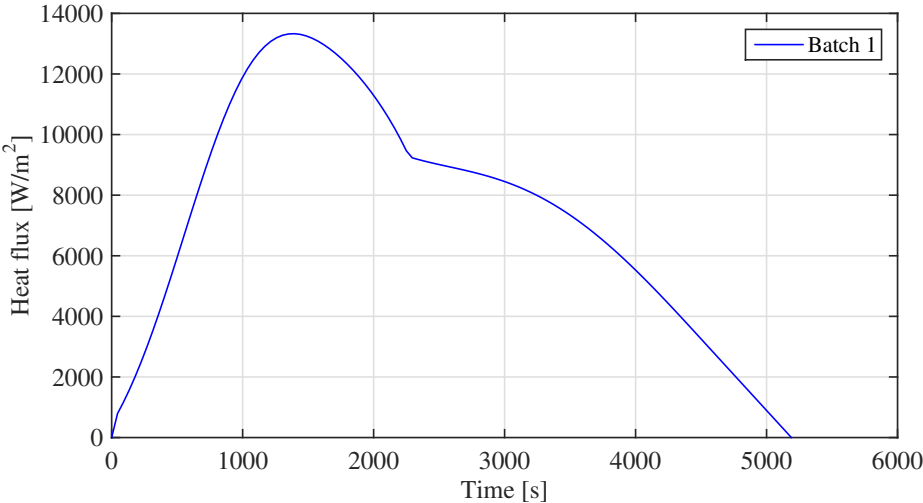


Figure 5.3: Heat flux from the wood stove supplied to the PCM heat storage unit.

A second batch of wood was added to the wood stove after 1 hour, where Figure 5.4 shows the combined heat flux

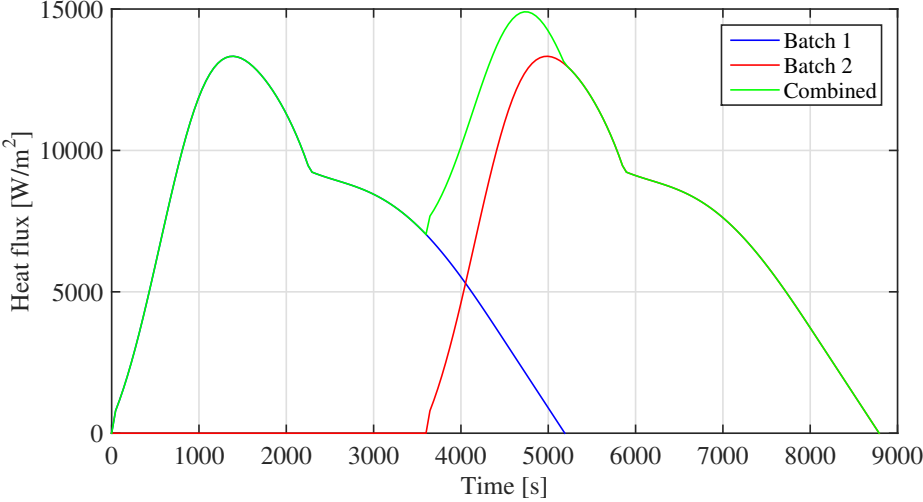


Figure 5.4: Heat flux from two batches of wood supplied to the PCM heat storage unit.

CHAPTER 5. OVERALL PCM HEAT STORAGE MODEL

In Chapter 3 an optimum fin geometry for heat rejection from the heat storage unit to the surroundings was found. The optimal dimensions of the fin channel were found to be a fin height of 15 mm and a fin spacing of 14 mm. Based on the results the convective heat transfer coefficient for the fin channel array to the surroundings was found. The convective heat transfer coefficient was calculated using the heat flux from Figure 3.11 with a surface temperature of 120°C and Equation 5.1

$$h = \frac{q}{(T_m - T_\infty)} \quad (5.1)$$

where

h	W/m ² K	thermal conductivity
q	W/m ²	heat flux
T_m	K	melting temperature
T_∞	K	surrounding/Inlet temperature

Figure 5.5 shows the convective heat transfer coefficient. It is a function of temperature, and it increases with increasing temperatures. The heat transfer coefficient is used as boundary condition on the cold surface of the PCM heat storage unit.

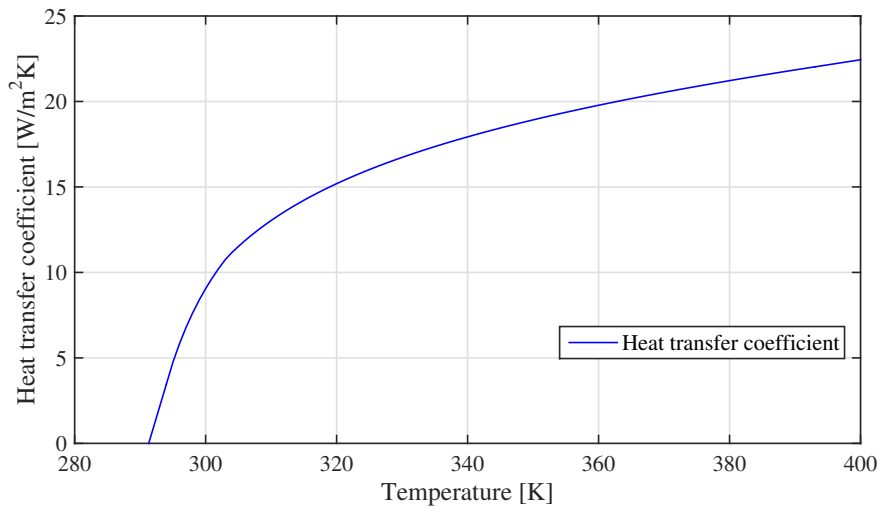


Figure 5.5: Heat transfer coefficient used as boundary condition on cold surface of heat storage unit.

As previously mentioned the moving boundary of the melting front must be able to move forward and backward according to the position of the melting front. Problems occurred with the model when the melting front ought to move back to the starting position when the PCM was solidifying. Because the temperature at the melting front had to be 118°C for the boundary to move, a condition was set to the velocity (See Equation 4.2 and 4.3) of the boundary so that if the temperature at the melting front was below the melting

temperature the velocity was set to zero. The problem therefore occurred when the heat flux of the wood combustion was decreasing and the temperature at the hot surface was decreased below the melting temperature. The problem was solved by changing the initial value of the model by obtaining the temperature profile for the length of the heat storage unit at the point where the hot surface of the heat storage unit had reached the melting temperature. The model was then started at the time where the temperature profile reached the melting temperature.

5.3 PCM

The effective thermal conductivity for liquid erythritol was found from the experiment where the heat storage unit was heated from below and was presented in Section 4.6. The effective thermal conductivity of liquid erythritol was found for a horizontal melting front. It was assumed that the effective thermal conductivity for liquid PCM obtained for a horizontal melting front is similar to the effective thermal conductivity of a vertical melting front. Figure 5.6 shows the effective thermal conductivity for liquid erythritol presented in Section 4.6. The effective thermal conductivity was used as material data for the conductivity of liquid erythritol in the model. Table 4.3 shows the material properties of erythritol used in the simulations.

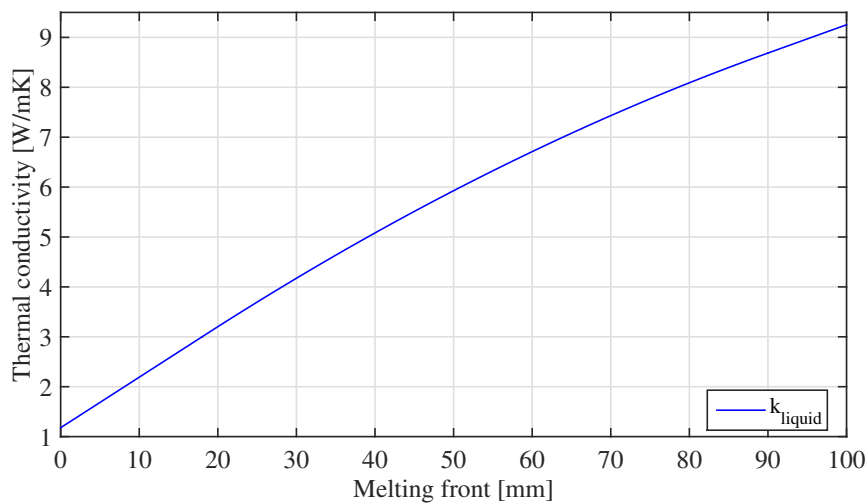


Figure 5.6: Effective thermal conductivity of liquid erythritol

5.4 PCM with aluminium foam

The effective thermal conductivity of PCM can be improved with the use of fins or metal foam. By enhancing the thermal conductivity problems with excess heating can be avoided and it will be possible to achieve a good heat distribution within the PCM. Aluminium foam with a porosity of 95% was added to the PCM. Adding a material with a higher conductivity to the PCM and thereby enhancing the effective thermal conductivity of the material will cause a surplus heat storage to the PCM.

The effective thermal conductivity of the PCM containing aluminium foam was calculated according to the model of Calmidi and Mahajan [1]. They developed a model for the effective thermal conductivity of high porosity fibrous metal foams, where they presented a periodic structure of the metal foam in the shape of a hexagonal unit cell. They found an excellent fit between data and the predicted value obtained for an area ratio of $r = 0.09$. The reader is requested to see reference for more details. The model is presented as

$$k_{\text{eff}} = \left(\frac{2}{\sqrt{3}} \left(\frac{r \left(\frac{b}{L} \right)}{k_f + \left(1 + \frac{b}{L} \right) \frac{k_{\text{por}} - k_f}{3}} + \frac{(1-r) \left(\frac{b}{L} \right)}{k_f + \frac{2}{3} \left(\frac{b}{L} \right) (k_{\text{por}} - k_f)} + \frac{\frac{\sqrt{3}}{2} - \frac{b}{L}}{k_f + \frac{4r}{3\sqrt{3}} \left(\frac{b}{L} \right) (k_{\text{por}} - k_f)} \right) \right)^{-1} \quad (5.2)$$

where b/L is

$$\frac{b}{L} = \frac{-r + \sqrt{r^2 + \frac{2}{\sqrt{3}}(1-\varepsilon) \left(2 - r \left(1 + \frac{4}{\sqrt{3}} \right) \right)}}{\frac{2}{3} \left(2 - r \left(1 + \frac{4}{\sqrt{3}} \right) \right)} \quad (5.3)$$

and

k_{eff}	W/mK	effective thermal conductivity
k_{por}	W/mK	thermal conductivity of porous media
k_f	W/mK	thermal conductivity of fluid
ε	–	porosity
r, b, L	–	dimension of unit-cell geometry. See reference [1].

Calculation of material properties of erythritol including aluminium with a porosity of 95% is presented in Appendix A.2 where the values from Table 4.3 was used as nominal values for erythritol. Table A.5 shows the properties of erythritol including aluminium foam.

5.5 Results and discussion

The results obtained from numerical simulations had two main requirements to fulfill. The temperature from the wood stove to the heat storage unit, and also the temperature leaving the heat storage unit should not exceed 150°C to keep the PCM from degrading. The required heat transfer rate from the fin channel arrangement to the surroundings was 2200 W/m^2 or more.

5.5.1 Heat storage unit heated with one batch of wood

Figures 5.7 – 5.10 shows various results obtained from the simulations where the heat storage unit was heated with one batch of wood. The results shows a comparison of results obtained using a PCM as well as a PCM with aluminium foam.

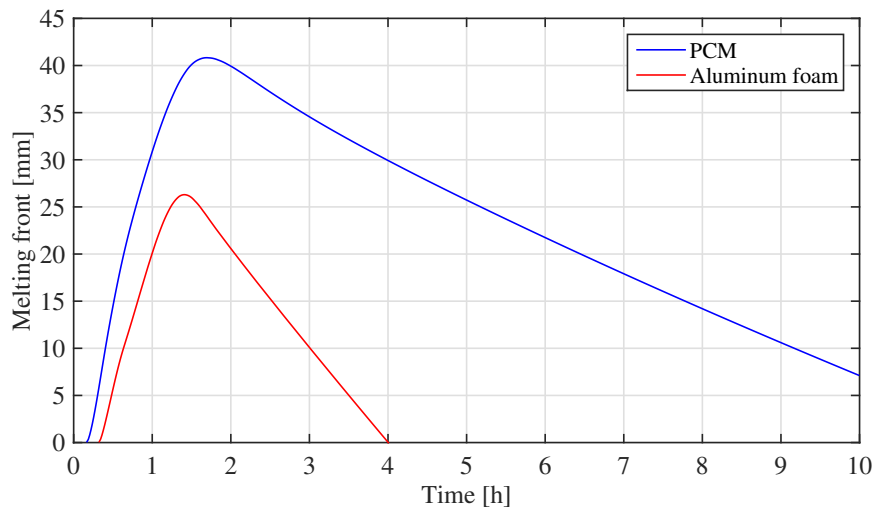


Figure 5.7: Melting front position in a storage unit heated with one batch of wood.

Figure 5.7 shows the position of the melting front in the heat storage unit, and how much PCM was melted at a given time. Since the length of the heat storage is 100 mm, both cases show that a small amount of PCM had melted compared to the total length of the heat storage unit. This indicates that the temperature distribution in the heat storage unit was not sufficient. The figure shows that approximately 41% (or 41 mm) was melted for PCM and approximately 27% (or 27 mm) for PCM with aluminium foam.

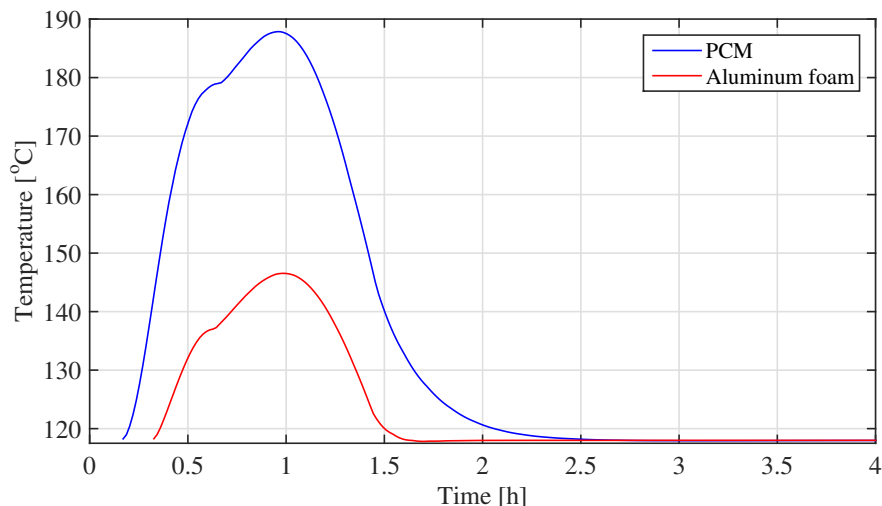


Figure 5.8: Temperature at hot surface for a storage unit heated with one batch of wood.

Figure 5.8 shows the temperature at the hot surface of the PCM heat storage unit. The figure shows that for the PCM the temperature exceeds the critical temperature of 150°C . For the PCM with aluminium foam the temperature was below the critical temperature, and the requirement was fulfilled.

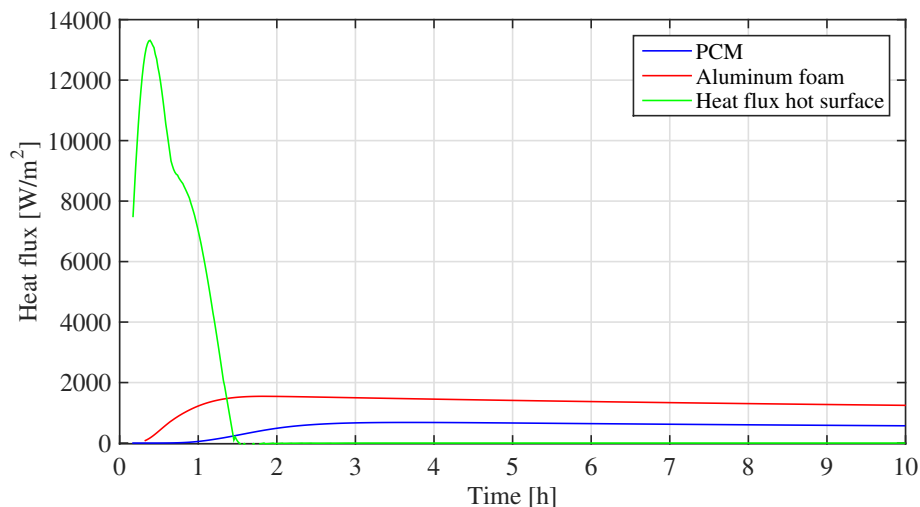


Figure 5.9: Heat flux for a storage unit heated with one batch of wood.

Figure 5.9 shows the heat flux at the cold surface of the heat storage unit. The figure shows a comparison of PCM and PCM with aluminium foam compared to the heat flux at the hot surface. The figure shows that the heat flux for the PCM with aluminium foam is higher than the heat flux from the PCM. Neither cases fulfill the requirement of heat transfer to the surroundings of 2200 W/m^2 .

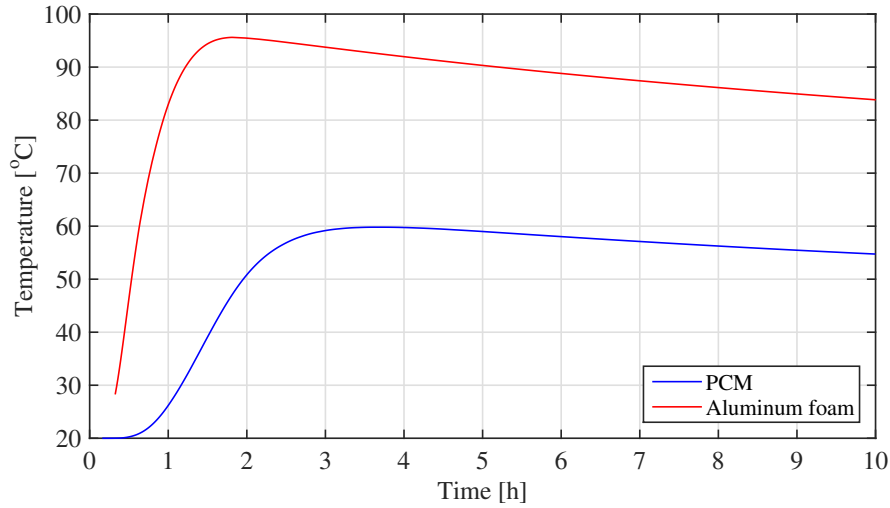


Figure 5.10: Temperature at cold surface for a storage unit heated with one batch of wood.

Figure 5.10 shows the temperature at the cold surface of the heat storage unit. The figure shows that the temperature of the PCM with aluminium foam has reached the highest temperature. Compared to the temperature at hot surface it was found that the time from the heat is supplied to the heat storage it takes about 1.5 hours before the temperature at hot surface has reached its maximum. The results also show that the temperature response is faster for the PCM with aluminium foam. Both temperatures were within the requirement of 150°C.

5.5.2 Heat storage unit heated with two batches of wood

A second batch of wood was added to the heat storage unit after 1 hour. Figures 5.11 – 5.14 show a comparison of heating with one batch of wood and heating with two batches of wood. The results presented are for PCM with aluminium foam only.

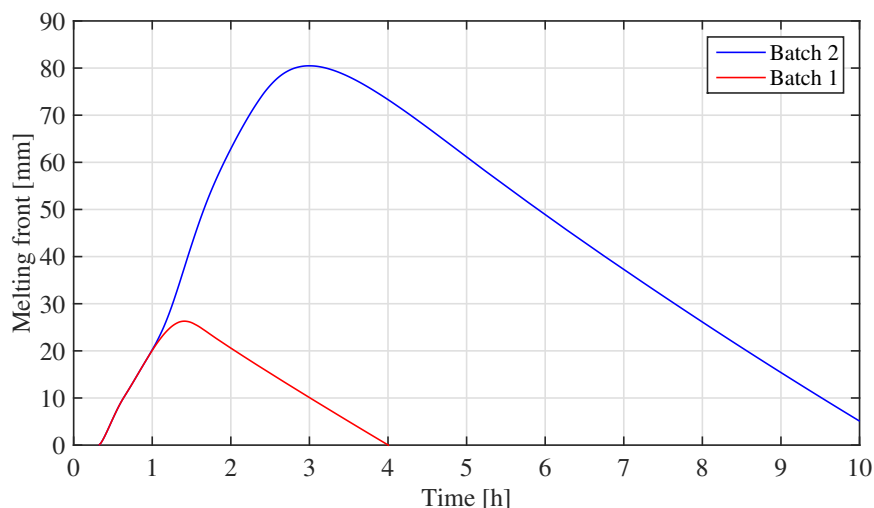


Figure 5.11: Melting front position in a storage unit utilizing PCM with aluminium foam, heated with two batches of wood.

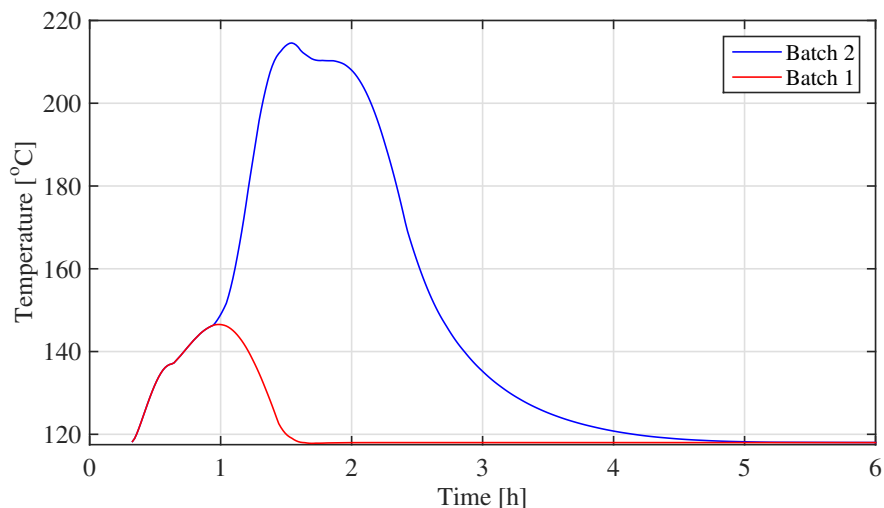


Figure 5.12: Temperature at hot surface for a storage unit utilizing PCM with aluminium foam, heated with two batches of wood.

Figure 5.11 shows the position of the melting front of the PCM in the heat storage unit. The figure shows that the melting front is more than three times as long for two batches of wood compared to the case with one batch of wood. Figure 5.12 shows the temperature at the hot surface of the PCM heat storage unit. When heating with one batch of wood the results show that the temperature at the hot surface does not exceed that of the

requirements. Heating with two batches of wood increase the temperature to a level significantly higher than the critical temperature.

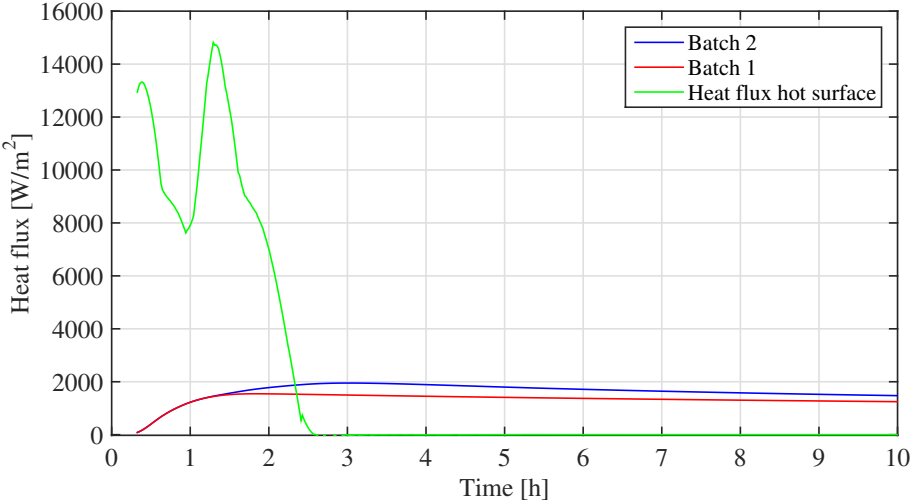


Figure 5.13: Heat flux for a storage unit utilizing PCM with aluminium foam, heated with two batches of wood.

Figure 5.13 shows the heat flux at the cold surface of the heat storage unit. A comparison of the results shows that the heat flux from the cold surface to the surroundings does not increase significantly when heating with two batches of wood. Even though Figures 5.11 and 5.12 show that the melting front position and the temperature at the hot surface have increased significantly, the heat transfer rate to the surroundings had not been affected to the same extent.

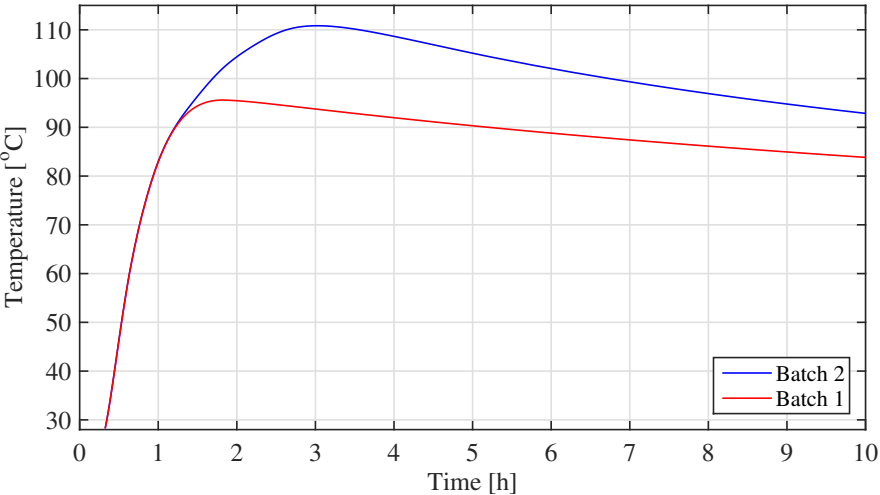


Figure 5.14: Temperature at cold surface for a storage unit utilizing PCM with aluminium foam, heated with two batches of wood.

Figure 5.14 shows the temperature at cold surface of the heat storage unit. The results show that the temperature has increased, and that it takes 3 hours before the temperature

at hot surface has reached its maximum. The temperature increase is much smaller than the temperature increase obtained at the hot surface of the heat storage unit.

5.5.3 Optimisation of the PCM heat storage unit

The results previously presented show that the heat storage unit does not fulfill the requirements set for temperatures and heat transfer rate from the heat storage unit to the surroundings. Two different approaches were tested in order to improve the performance of the heat storage unit. Results for the heat storage unit heated with one batch of wood showed that less than half of the PCM in the heat storage unit had melted. Based on this result it was decided to halve the length of the storage unit from 100 mm to 50 mm. The second approach that was studied was halving the heat flux, and increase the burning duration by twofold for one batch of wood. The results covers only the use of PCM with aluminium foam.

Figures 5.15 – 5.18 show various results for a heat storage unit with a length of 50 mm heated with one batch of wood. The results are compared to results for a heat storage unit with a length of 100 mm. Figure 5.15 shows the melting front in the heat storage unit. The figure shows that approximately 72% (36 mm out of 50 mm) of the PCM had melted. Compared to approximately 27% for the heat storage unit with a length of 100 mm. This shows a significant increase.

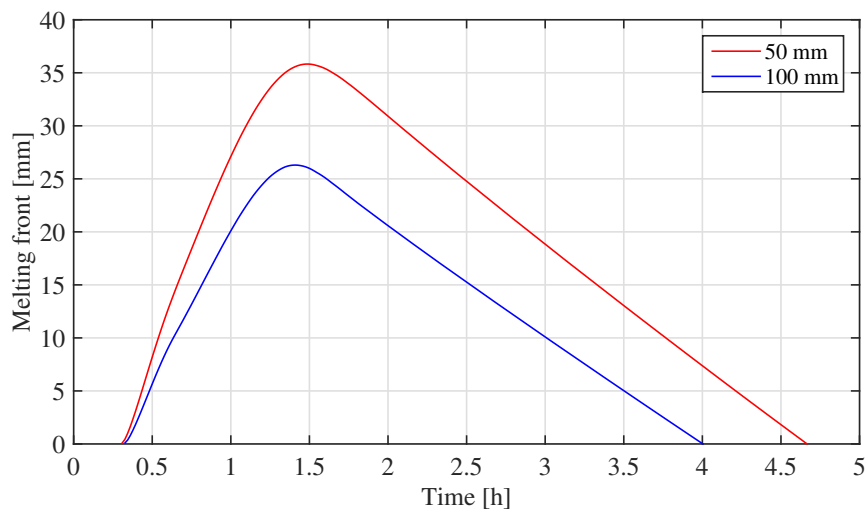


Figure 5.15: Melting front for a storage unit with a length of 50 mm.

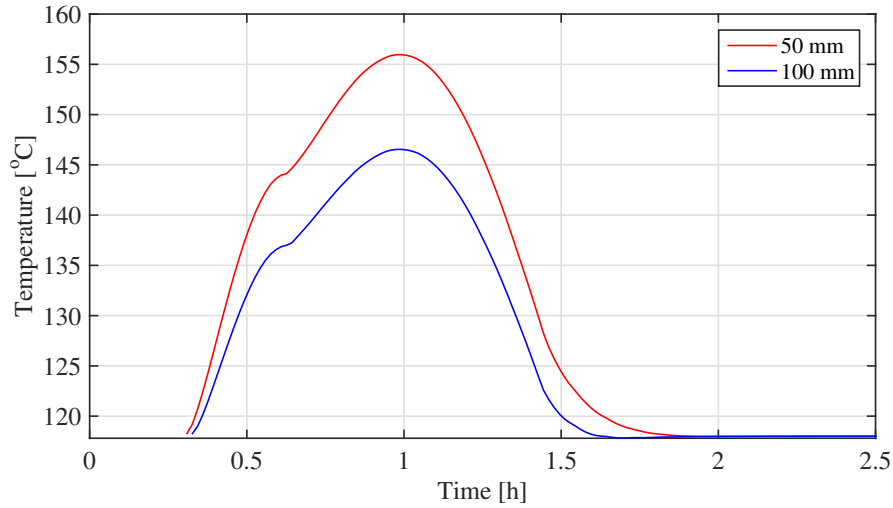


Figure 5.16: Temperature at hot surface for a storage unit with a length of 50 mm.

Figure 5.16 shows the temperature at the hot surface of the heat storage unit. The figure shows that the temperature had increased above the critical temperature. Compared to the heat storage unit with a length of 100 mm, the temperature increased by approximately 10°C .

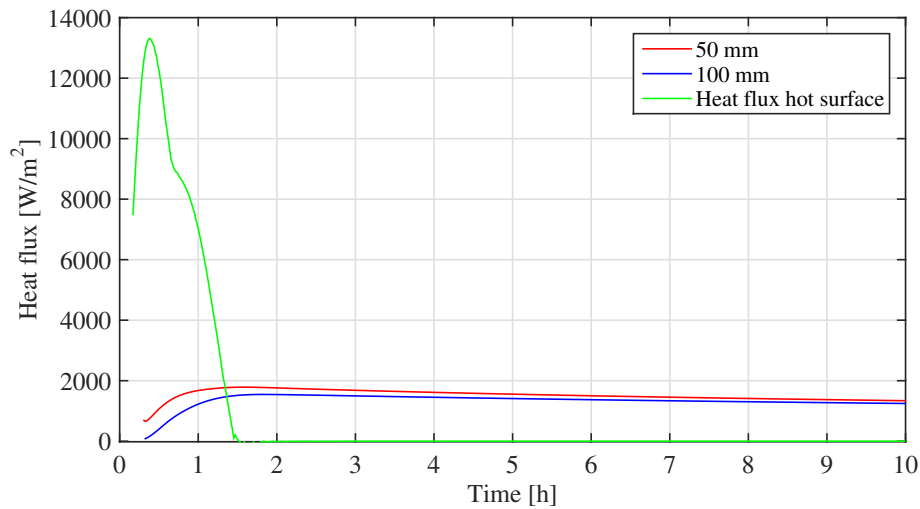


Figure 5.17: Heat flux for a storage unit with a length of 50 mm.

Figure 5.17 shows the heat flux for the heat storage unit. The figure shows that the heat flux from the storage unit to the surroundings does not fulfill the requirement of 2200 W/m^2 . Compared to results for the heat storage with a length of 100 mm, the heat flux did not increase significantly.

Figure 5.18 shows the temperature at the cold surface of the heat storage unit. Compared to results from the heat storage unit with a length of 100 mm, the temperature shows an increase of about 10°C.

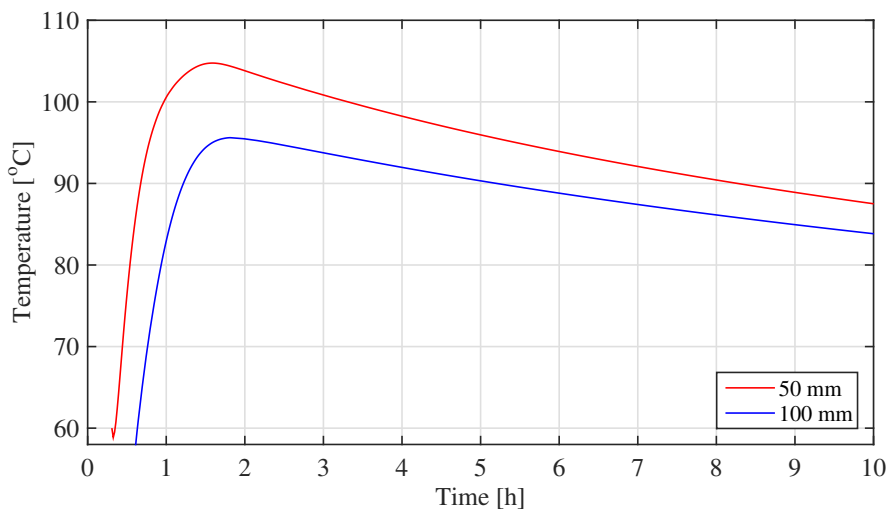


Figure 5.18: Temperature at cold surface for a storage unit with a length of 50 mm.

The heat flux was halved and the burning duration doubled for the new approach. Figures 5.19 – 5.22 show various results for the heat storage unit heated with the new heat flux. The results show a comparison of two heat storage units with different lengths. The length of the heat storage units are 100 mm and 50 mm. The figures show results for PCM with aluminium foam only.

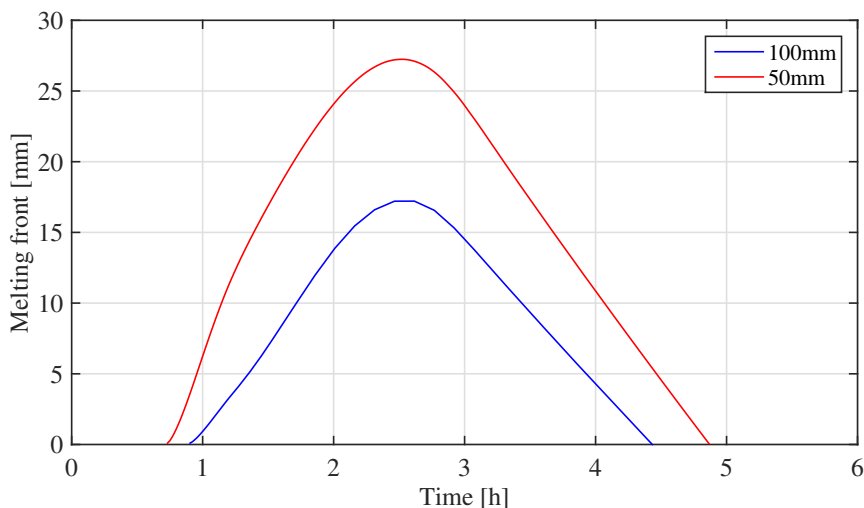


Figure 5.19: Melting front for two heat storage units with a length of 100 mm and 50 mm.

Figure 5.19 shows the melting front position for the two heat storage units with different lengths. The comparison show that the storage unit with a length of 50 mm had melted the most.

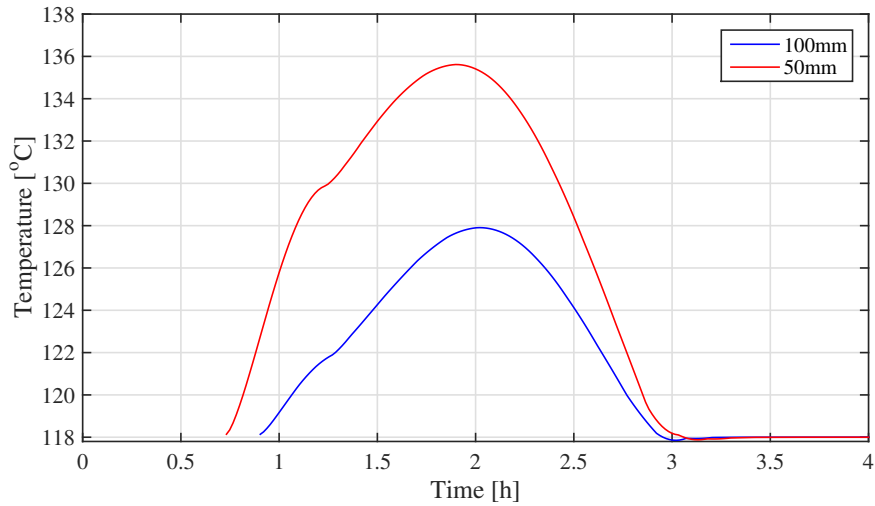


Figure 5.20: Temperature at hot surface for two heat storage units with a length of 100 mm and 50 mm.

Figure 5.20 shows the temperature at the hot surface. The comparison show that the storage unit with a length of 50 mm reached a higher temperature than the storage unit with a length of 100 mm. The results show that the temperature obtained for both heat storage units is within the required temperature of 150°C.

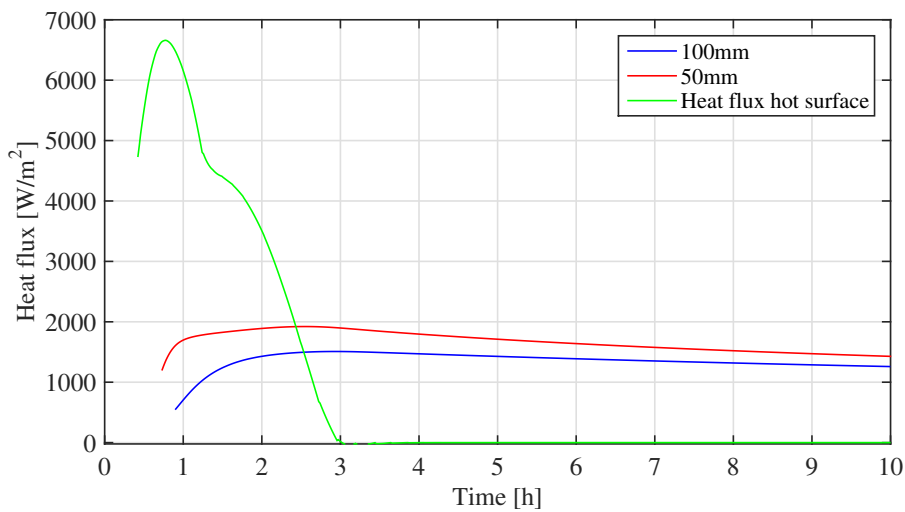


Figure 5.21: Heat flux for two heat storage units with a length of 100 mm and 50 mm.

Figure 5.21 shows the heat flux for the two heat storage units. The results show that the heat flux from the heat storage unit with a length of 50 mm is higher than the heat flux for the heat storage unit with a length of 100 mm. Neither of the heat storage units fulfill the required rate of heat transfer to the surroundings.

Figure 5.22 shows the temperature at the cold surface for the two heat storage units. The comparison show that the temperature for the heat storage unit with a length of 50 mm is higher than for the storage unit with a length of 100 mm.

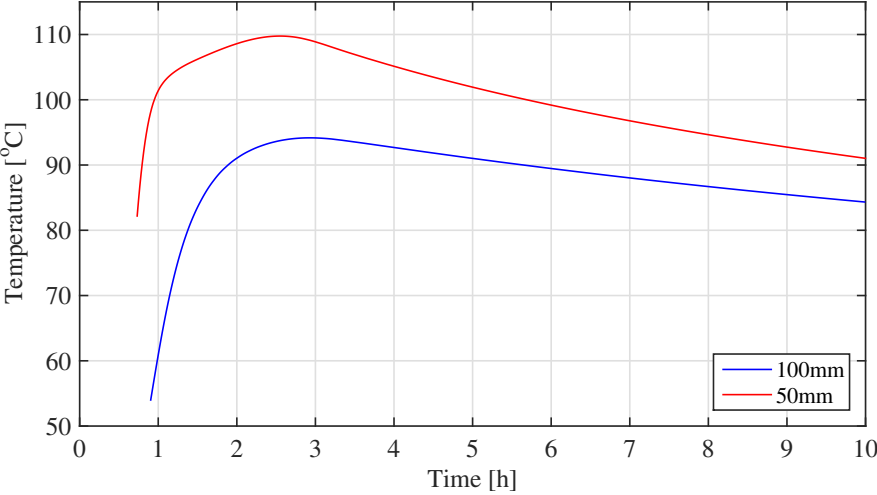


Figure 5.22: Temperature at cold surface for two heat storage units with a length of 100 mm and 50 mm.

5.6 Summary, conclusions and discussion

An overall heat storage model was developed to combine heat supply, storage and distribution. The simulations were carried out with PCM and PCM with aluminium foam to enhance the heat distribution in the heat storage unit and the heat transfer rate to the surroundings. The aluminium foam had a porosity of 95%. A heat flux based on calculations of batch combustion of wood was supplied from the wood stove to the heat storage unit. A convective heat transfer coefficient based on the fin arrangement found in Chapter 3 was used as boundary condition on cold surface, and the effective thermal conductivity for liquid erythritol from Chapter 4 was used.

The results obtained included the position of the melting front, temperature at the hot surface, temperature at the cold surface and the heat flux from the storage unit rejected to the surroundings. The results showed that about 41% of the PCM melted compared to 27% of PCM with aluminium foam. This is a surprisingly low amount of melted PCM considering the length of the storage unit. The temperatures obtained at hot and cold surfaces for PCM with aluminium foam were both below the critical temperature of 150°C. The heat flux rejected to the surroundings, however, did not reach the required rate of heat transfer of 2200 W/m².

After 1 hour a second batch of wood was added to the heat storage unit. This simulation considered only PCM with aluminium foam. This time 80% of the PCM in the storage unit melted. The temperature at the hot surface increased beyond the critical temperature of 150°C. The heat flux rejected to the surroundings did not increase significantly compared to a storage unit heated with one batch of wood.

An optimisation of the heat storage unit was conducted. A first approach was to halve the length of the storage unit to 50 mm, since a storage unit with a length of 100 mm proved to be excess to requirements. A second approach was to halve the heat flux and increase the burning time by twofold.

For all the obtained results the heat transfer to the surroundings was not fulfilled according to the requirements, and the length of the PCM heat storage was proved to be excessive.

Chapter 6

Summary, conclusions and recommendations

6.1 Summary and conclusions

Methods for enhancing the heat transfer from a PCM heat storage unit to the surroundings were studied. The studies considered both free convection and radiation heat transfer. The objective was to find a suitable fin geometry for heat rejection to the surroundings. Based on the study it was concluded that a fin channel was the best choice prior to the fin array. Calculations showed that with a fin height of 15 mm, a fin spacing of 14 mm and a base-to-ambient temperature difference of 100°C the geometry would meet the requirements of heat transfer by 2200 W/m² to the surroundings. It was however found that with a decreasing base-to-ambient temperature difference the heat transfer to the surroundings would decrease significantly.

A PCM heat storage unit was investigated experimentally. The experiments considered two different setups, supplying heat to the heat storage units top surface and supplying heat to the bottom surface. The results from the experiment where the heat storage unit was heated from the top surface showed that only 30% of the PCM inside the storage unit had melted after 25 hours. Comparing temperatures and position of the thermocouples to numerical simulations however showed good agreement with an average relative error of 0.8%. The heat storage unit heated from below proved that heat transfer by free convection in the liquid phase had a significant impact on the melting pace of the PCM. All PCM inside the heat storage unit had melted after 18 hours. The comparison of results from the experiments with numerical simulations did however not show an immediate agreement or similar behaviour.

The effective thermal conductivity of erythritol was estimated based on the experiments.

An uncertainty analysis was performed on the obtained effective conductivity. The results from the uncertainty analysis showed that the uncertainty of the effective thermal conductivity obtained from the experiment where the heat storage unit was heated from the top had the highest uncertainty of 31%. It was concluded that the method employed for studying the effective thermal conductivity was inaccurate.

An overall heat storage model was developed to combine heat supply, storage and distribution. The simulations were performed using PCM as well as PCM with aluminium foam to enhance the heat distribution in the heat storage unit and the heat transfer rate to the surroundings. The results from the first simulations showed that a heat storage unit containing PCM only had melted 41% compared to 27% for PCM with aluminium foam, and the temperature at hot surface was within the requirements of 150°C. The heat transfer from cold surface to the surroundings showed that neither PCM nor PCM with aluminium foam had reached the required value of 2200 W/m². An optimization of the heat storage unit was performed. Because the size of the PCM heat storage unit was proved to be excessive, the optimization included halving the length of the PCM heat storage from 100 mm to 50 mm. The other approach was to double the burning duration and halving the heat flux. The results showed that the heat storage unit did not fulfill the requirement of heat transfer to the surroundings for any of the improvements made.

6.2 Recommendations for further work

The experimental setup of a heat storage unit heated from below proved that free convection heat transfer in the liquid phase had a significant impact on the melting phase of the PCM. The results compared to numerical simulations did however not show an immediate agreement. Heat transfer with free convection is very beneficial and should be investigated with more experiments, preferably in combination with a wood stove. Because the comparison with numerical simulations did not show similar behaviour, a new and improved numerical model should be developed for better comparison of the results from experiments.

The overall heat storage model showed the most disappointing results. The model did show interesting and to some extent good results, but none of the models tested or the implemented improvements caused the model to fulfill the requirements of heat transfer by 2200 W/m^2 . Specific proposals for improvement are to optimize the length of the heat storage unit. By optimizing the length, more of the PCM can be melted and more heat can be stored as latent heat. The fin channel geometry at the outer surface could be dimensioned for a base-to-ambient temperature difference of less than 100°C . By overdimensioning the heat transfer from the fin geometry the heat transfer from the heat storage unit could be enhanced. The aluminium foam inside the heat storage unit could be adapted or replaced with aluminium fins. Different arrangements of the aluminium inside the heat storage could be investigated to obtain a better heat distribution in the heat storage unit. If the aluminium arrangements were placed at the beginning of the heat storage, keeping a distance of PCM only at the cold surface, the heat transfer inside the heat storage unit would be fast, the heat distribution good, and the heat transfer from the heat storage unit to the surroundings slower.

Bibliography

- [1] V. V. Calmidi and R. L. Mahajan. The effective thermal conductivity of high porosity fibrous metal foams. *J. Heat Transfer*, 121(2):466 – 471, 1999.
- [2] COMSOL. Heat transfer module user’s guide. <http://www.ewp.rpi.edu/hartford/~collir5/MP/OTHER/Reference/HeatTransferModuleUsersGuide.pdf>, 1998 – 2012. [Retrieved 13 February 2015].
- [3] A. Güvenç and H. Yüncü. An experimental investigation on performance of fins on a horizontal base in free convection heat transfer. *Heat and Mass Transfer*, 37:409 – 416, 2001.
- [4] G. F. Hewitt. *Heat exchanger design handbook*. Begell House, 2002.
- [5] Incropera, DeWitt, Bergmann, and Lavine. *Fundamentals of heat and mass transfer*. John Wiley & Sons, 2007.
- [6] D.W. Mueller Jr. and H.I. Abu-Mulaweh. Prediction of the temperature in a fin cooled by natural convection and radiation. *Applied Thermal Engineering*, 26(14–15):1662 – 1668, 2006.
- [7] Murat Kenisarin and Khamid Mahkamov. Solar energy storage using phase change materials. *Renewable and Sustainable Energy Reviews*, 11(9):1913 – 1965, 2007.
- [8] Harald Mehling and Luisa F. Cabeza. *Heat and cold storage with PCM*. Springer, 2008.
- [9] Robert J. Moffat. Describing the uncertainties in experimental results. *Experimental Thermal and Fluid Science*, 1(1):3 – 17, 1988.
- [10] V. Rammohan Rao and S.P. Venkateshan. Experimental study of free convection and radiation in horizontal fin arrays. *International Journal of Heat and Mass Transfer*, 39(4):779 – 789, 1996.
- [11] E.M. Sparrow and S.B. Vemuri. Orientation effects on natural convection/radiation heat transfer from pin-fin arrays. *International Journal of Heat and Mass Transfer*, 29(3):359 – 368, 1986.

BIBLIOGRAPHY

- [12] StableWood. Project summary. <http://www.sintef.no/Projectweb/StableWood/Project-summary/>, 2011. [Retrieved 6 February 2015].
- [13] Anthony J. Wheeler and Ahmad R. Ganji. *Introduction to Engineering Experimentation*. Pearson Education, Inc., 2004.
- [14] B. Yazicioğlu and H. Yüncü. Optimum fin spacing of rectangular fins on a vertical base in free convection heat transfer. *Heat and Mass Transfer*, 44(1):11 – 21, 2007.
- [15] Kristin Sveine Ytredal. Investigation of heat storage in future wood stoves. Project work, Norwegian University of Science and Technology, 2014.

Appendix A

Data

A.1 Material properties

Table A.1: Material properties of teflon

Properties	Value	Unit
Thermal conductivity	0.25	W/mK
Specific heat capacity	1300	J/kgK
Density	2160	kg/m ³

Table A.2: Material properties of silcapor

Properties	Value	Unit
Thermal conductivity	0.02	W/mK
Specific heat capacity	733	J/kgK
Density	280	kg/m ³

Table A.3: Material properties of Erythritol

Properties	Expression	Value	Unit
Molecular formula	–	C4H10O4	–
Molecular mass	–	122.12	g/mol
Melting temperature	T_m	118	°C
Max temperature	T_{max}	160	°C
Latent heat	H_{sl}	339.8	kJ/kg
Specific heat capacity, solid	C_{ps}	1380	J/kgK
Specific heat capacity, liquid	C_{pl}	2760	J/kgK
Thermal conductivity, solid (20 °C)	k_s	0.733	W/mK
Thermal conductivity, liquid (140 °C)	k_l	0.326	W/mK
Density, solid	ρ_s	1480	kg/m ³
Density, liquid	ρ_l	1300	kg/m ³

A.2 Material properties of erythritol with aluminium foam with a porosity of 95%

Table A.4: Material properties of aluminum [5]

Variable	Expression	Value	Unit
Thermal conductivity	k	237	W/mK
Specific heat capacity	C_p	903	J/kgK
Density	ρ	2702	kg/m ³

Density

$$\rho_{\text{tot}} = \frac{\rho_{(\text{PCM})}V_{(\text{PCM})} + \rho_{(\text{al})}V_{(\text{al})}}{V_{\text{tot}}} = \rho_{(\text{PCM})}\varepsilon + \rho_{(\text{al})}(1 - \varepsilon) \quad (\text{A.1})$$

$$V_{(\text{PCM})} = \varepsilon V_{\text{tot}} \quad (\text{A.2})$$

$$V_{(\text{al})} = (1 - \varepsilon)V_{\text{tot}} \quad (\text{A.3})$$

$$V_{\text{tot}} = \pi r^2 h \quad (\text{A.4})$$

where

ρ	kg/m ³	Density
V	m ³	Volume
ε	–	Porosity

Specific heat capacity

$$C_{p\text{tot}} = \frac{C_{p(\text{PCM})}m_{(\text{PCM})} + C_{p(\text{al})}m_{(\text{al})}}{m_{\text{tot}}} \quad (\text{A.5})$$

where

C_p	J/kgK	Specific heat capacity
m	kg	Mass

Latent heat

$$H_{sl} = \frac{H_{sl(\text{PCM})}m_{(\text{PCM})}}{m_{\text{tot}}} \quad (\text{A.6})$$

$$H_{sl(\text{tot})} = \frac{H_{sl(s)} + H_{sl(l)}}{2} \quad (\text{A.7})$$

where

H_{sl}	kJ/kg	Latent heat
m	kg	Mass

Table A.5: Properties of erythritol including aluminium foam with a porosity of 95%

Variable	Expression	Value	Unit
Effective thermal conductivity, solid	$k_{\text{eff}-s}$	5.31	W/mK
Effective thermal conductivity, liquid	$k_{\text{eff}-l}$	4.85	W/mK
Latent heat	H_{sl}	308	kJ/kg
Density, solid	ρ_s	1541	kg/m ³
Density, liquid	ρ_l	1349	kg/m ³
Specific heat capacity, solid	C_{ps}	1624	J/kgK
Specific heat capacity, liquid	C_{pl}	2945	J/kgK

Appendix B

Net heat storage capacity

A numerical model was developed to calculate the total internal energy in the heat storage unit. The boundary condition at hot and cold surface was 150°C and 94°C, respectively. The temperatures was obtained from TT13 and TT15 at steady state. A 1D model was developed. The model considered heat transfer with phase change, and was simulated untill reached steady state. Table B.1 show the total internal energy obtained from Comsol Multiphysics at steady state and ambient.

Table B.1: Net heat storage capacity found using Comsol

Variable	Expression	Value	Unit
Total internal energy at S.S.	E_{SS}	302.5	kJ/kg
Total internal energy at 20°C	E_{amb}	-8.5	kJ/kg
Total internal energy	ΔE	311	kJ/kg

Table 4.3 shows the material properties used. Because erythritol expand with 10% when liquid the mean density was calculated and used in the simulations, where $\rho_m = 1379$ kg/m³. The melting front position was found from the temperature profile in the simulations, where the position of the melting front, S , was 41 mm and considered uniform.

$$V_{tot} = \frac{\pi D^2 h}{4} \quad V_{melt} = \frac{\pi S^2 h}{4} \quad V_{sol} = V_{tot} - V_{melt} \quad (B.1)$$

$$m_{tot} = V_{tot} \cdot \rho_m \quad m_{melt} = V_{melt} \cdot \rho_m \quad m_{sol} = V_{sol} \cdot \rho_m \quad (B.2)$$

Net heat storage capacity was calculated based on Table B.1 and Equations B.1 and B.2. The amount of latent heat was calculated according to equation B.3.

$$E_{\text{melt}} = H_{sl} \cdot m_{\text{melt}} \quad (\text{B.3})$$

Table B.2: Net heat storage capacity from calculations

Variable	Expression	Value	Unit
Latent heat	E_{melt}	148.7	kJ
Sensible heat	E_{sol}	200.4	kJ

Table B.2 shows the amount of latent and sensible heat. The total internal energy determined from Comsol was 336.8 kJ. Where the total internal energy from calculations for latent and sensible heat was 349.1 kJ. This shows a difference of approximately 4%. The determining of the position of the melting front can be the reason for the deviation, as the calculations are quite sensitive on small variations.

Appendix C

Uncertainty analysis

The procedure of the uncertainty analysis is performed according to Moffat [9] and Wheeler and Ganji[13]. An uncertainty analysis is a process of determining the effect the uncertainties the measurements have on the calculated result. The analysis is only as good as the equations it is based on, and incomplete equations can underestimate the uncertainty on the result, but also overstating the error can overestimate the total uncertainty [9]. The larger the uncertainties are, the more it will dominate the result. Reducing the uncertainty on the calculated result can be gained more effectively by reducing one single large error than reducing several small errors [13].

If X_i is a variable with a known uncertainty, ΔX_i , it may be presented by

$$X_i = X_i(\text{measured}) \pm \Delta X_i \quad (\text{C.1})$$

the result R of an experiment with a set of measurement will have an uncertainty in the calculated result, ΔR , such that

$$R = R(X_1, X_2, X_3, \dots, X_n) \pm \Delta R \quad (\text{C.2})$$

The uncertainty ΔR can be estimated with a root-sum-square equation considering all individual uncertainties

$$\Delta R = \sqrt{\sum_{i=1}^n \left(\frac{\partial R}{\partial X_i} \Delta X_i \right)^2} \quad (\text{C.3})$$

C.1 Uncertainties

A total of three different conductivities have been obtained, one for solid and two for liquid erythritol. Using the obtained value for the solid erythritol the conductivity of the liquid phase have been determined. One from the experiment where the heat storage where heated from the top and one from the experiment where the heat storage where heated from below.

Table C.1 show the uncertainty of the individual variables which influence the estimation of the thermal conductivities. The uncertainty in temperature of the thermocouple will either be $\pm 0.4\%$ for thermocouples that are not calibrated, or $0.3K$ for thermocouples that are calibrated. As the non-calibrated thermocouple can contribute to a significant difference in the temperatures of the thermocouples, the overall uncertainty of the liquid erythritol have been calculated concerning both uncertainties separately.

Table C.1: Uncertainties

Variable	Uncertainty
Hot disk instrument	$\pm 5.00\%$
Heat flux indicator	$\pm 3.00\%$
Non-calibrated thermocouple	$\pm 0.40\%$ (in K)
Calibrated thermocouple	$\pm 0.30K$
Melting front ($\pm 2\sigma$)	$\pm 4.18\%$
Melting temperature	$\pm 0.50K$
Position of thermocouple	$\pm 1.00mm$

Assuming a Gaussian distribution of the melting front parameter, S , the individual uncertainty is calculated as a standard deviation difference between the measured result and a curve-fit used as reference. The standard deviation is defined as

$$\sigma = \sqrt{\frac{1}{n-1} \sum_{j=1}^n (S_j - \bar{S})^2} \quad (C.4)$$

For a 95% confidence interval, the uncertainty is 2σ .

C.2 Conductivity of solid erythritol

Conductivity of solid erythritol is measured using a Hot Disk instrument. The conductivity is a function of temperature, where the uncertainty of the Hot Disk instrument is $\pm 5\%$. Table C.2 show the measured value of solid conductivity of erythritol and its uncertainty.

Table C.2: Uncertainty of solid erythritol

Variable	Value (W/mK)	Uncertainty
k_{solid}	0.78	$\pm 5\%$

C.3 Liquid conductivity: Experiment heated from the top

The liquid conductivity is obtained using a Matlab computer code and a model in Comsol Multiphysics developed by Kristjansson. The computer codes works as a black box where the uncertainties of each individual parameter is calculated separately. The nominal value of liquid conductivity is 0.40 W/mK. Table C.4 show the uncertainty of each individual parameter, and table C.5 show the uncertainty of the liquid conductivity.

$$q_s = \frac{2\pi L k_{silcapor}}{\ln(r_o/r_i)} \frac{4}{D^3\pi} \quad (C.5)$$

where

q_s	W/m ³ K	Volumetric heat loss
$k_{silcapor}$	W/mK	Conductivity of slicapor
L	m	Length of heat storage
r_o	m	Outer radius
r_i	m	Inner radius
D	m	Diameter of heat storage

$$\frac{\Delta q_s}{q_s} = \sqrt{\left(\frac{\Delta L}{L}\right)^2 + \left(\frac{\Delta r_o}{r_o}\right)^2 + \left(\frac{\Delta r_i}{r_i}\right)^2 + \left(\frac{\Delta D}{D}\right)^2} \quad (C.6)$$

Table C.3: Nominal values and individual uncertainties for q_s

Variable	Nominal value	Unit	Expression	Individual uncertainty
q_s (0 – 25mm)	8.872	W/m ³ K	–	–
q_s (25 – 100mm)	14.298	W/m ³ K	–	–
$k_{silcapor}$	0.020	W/mK	–	–
L	0.100	m	$\Delta L/L$	0.7223
r_o	0.224	m	$\Delta r_o/r_o$	0.6521
r_i	0.074	m	$\Delta r_i/r_i$	0.6521
D	0.100	m	$\Delta D/D$	–2.1669

APPENDIX C. UNCERTAINTY ANALYSIS

Table C.4: Individual uncertainties of liquid conductivity from black box

Variable	Uncertainty	k_l^+	k_l^-	$k_{nom} - k_l^+$	$k_{nom} - k_l^-$	max	$(\Delta k_l/k_l)_x$
k_{solid}	$\pm 5.0\%$	0.43	0.40	0.03	0.00	0.03	0.075
C_p	$\pm 5.0\%$	0.43	0.41	0.03	0.01	0.03	0.075
ρ	$\pm 1.0\%$	0.41	0.39	0.01	0.01	0.01	0.025
Non-cal. T_h	$\pm 0.4\%$	0.41	0.42	0.01	0.02	0.02	0.050
Calibrated T_h	$\pm 0.3\text{K}$	0.40	0.43	0.00	0.03	0.03	0.075
Pos. of TT01	$\pm 1\text{mm}$	0.48	0.37	0.08	0.03	0.08	0.200
Pos. of TT02	$\pm 1\text{mm}$	0.40	0.41	0.00	0.01	0.01	0.025
Pos. of TT03	$\pm 1\text{mm}$	0.40	0.41	0.00	0.01	0.01	0.025
Pos. of TT04	$\pm 1\text{mm}$	0.42	0.42	0.02	0.02	0.02	0.050
Pos. of TT05	$\pm 1\text{mm}$	0.41	0.43	0.01	0.03	0.03	0.075
Pos. of TT06	$\pm 1\text{mm}$	0.34	0.43	0.06	0.03	0.06	0.150
Pos. of TT07	$\pm 1\text{mm}$	0.42	0.40	0.02	0.00	0.02	0.050
Pos. of TT08	$\pm 1\text{mm}$	0.40	0.41	0.00	0.01	0.01	0.025
Pos. of TT09	$\pm 1\text{mm}$	0.42	0.41	0.02	0.01	0.02	0.050
q_s	$\pm 2.46\text{W/m}^3\text{K}$	0.42	0.40	0.02	0.00	0.02	0.050

$$\left. \begin{array}{l} |k_{nom} - k_l^+| \\ |k_{nom} - k_l^-| \end{array} \right\} \max \Rightarrow \left(\frac{\Delta k_l}{k_l} \right)_x = \frac{\partial k_l}{\partial x} \Delta x$$

$$\frac{\Delta k_l}{k_l} = \sqrt{\left(\frac{\Delta k_l}{k_l} \right)_{k_s}^2 + \left(\frac{\Delta k_l}{k_l} \right)_{C_p}^2 + \left(\frac{\Delta k_l}{k_l} \right)_{\rho}^2 + \left(\frac{\Delta k_l}{k_l} \right)_{T_h}^2 + \left(\frac{\Delta k_l}{k_l} \right)_{TT01}^2 + \dots} \quad (\text{C.7})$$

Table C.5: Uncertainty of liquid conductivity

Expression	Uncertainty	
	$T_h \pm 0.4\%$	$T_h \pm 0.3\text{K}$
$\Delta k_l/k_l$	30.7%	31.2%

C.4 Liquid conductivity: Experiment heated from below

The liquid conductivity from experiment where the heat storage where heated from below is calculated according to

$$k_l = \frac{qS}{(T_h - T_m)} \quad (\text{C.8})$$

where

k_l	W/mK	Liquid conductivity of erythritol
q	W/m ²	Heat flux
S	m	Melting front
T_h	K	Hot temperature
T_m	K	Melting temperature

From equation C.8 the uncertainty in liquid conductivity is expressed as

$$\frac{\Delta k_l}{k_l} = \sqrt{\left(\frac{\Delta q}{q}\right)^2 + \left(\frac{\Delta S}{S}\right)^2 + \left(\frac{\Delta T_h}{T_h}\right)^2 + \left(\frac{\Delta T_m}{T_m}\right)^2} \quad (\text{C.9})$$

Table C.6 show the measured nominal value for different time steps, table C.7 show the individual uncertainties for each time step, and table C.8 show the uncertainty and average uncertainty of liquid conductivity.

Table C.6: Measured nominal values for different time steps

Variable	Value	20000s	40000s	60000s
k_l	W/mK	3.7764	6.5260	8.5004
q	W/m ²	1523.0	1559.7	1472.1
S	m	0.0258	0.0570	0.0874
T_h	K	401.40	404.66	406.14
T_m	K	391.00	391.00	391.00

Table C.7: Individual uncertainties for liquid conductivity measurements

Variable	Expression	Uncertainty		
		20000s	40000s	60000s
q	$\Delta q/q$	0.1133	0.1952	0.2550
S	$\Delta S/S$	0.1579	0.2720	0.3553
$T_h \pm 0.4\%$	$\Delta T_h/T_h$	-0.5832	-0.7708	-0.9122
$T_h \pm 0.3K$	$\Delta T_h/T_h$	-0.1090	-0.1429	-0.1685
T_m	$\Delta T_m/T_m$	-0.1816	-0.2381	-0.2808

Table C.8: Uncertainty and average uncertainty of liquid conductivity

Time	Expression	Uncertainty	
		$T_h \pm 0.4\%$	$T_h \pm 0.3K$
20000s	$\Delta k_l/k_l$	16.97%	7.61%
40000s	$\Delta k_l/k_l$	13.38%	6.66%
60000s	$\Delta k_l/k_l$	12.35%	6.43%
Average uncertainty		14.23%	6.90%

Appendix D

Risk assessment

Risk Assessment Report

Stablewood- PCM Testrigg

Prosjektnavn	Stablewood
Apparatur	PCM testrigg
Enhet	NTNU-EPT
Apparaturansvarlig	Kolbeinn Kristjansson
Prosjektleder	Erling Næss
HMS-koordinator	Morten Grønli
HMS-ansvarlig (linjeleder)	Olav Bolland
Plassering	VATL
Romnummer	C165
Risikovurdering utført av	Kolbeinn Kristjansson

Approval:

Apparatur kort (UNIT CARD) valid for:	
Forsøk pågår kort (EXPERIMENT IN PROGRESS) valid for:	

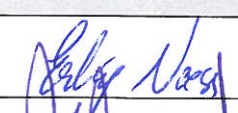
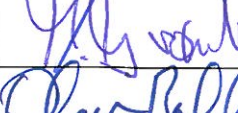

Rolle	Navn	Dato	Signatur
Prosjektleder	Erling Næss	2014-08-05	
HMS koordinator	Morten Grønli	7/7-2014	
HMS ansvarlig (linjeleder)	Olav Bolland	13/8-2014	

TABLE OF CONTENTS

1	INTRODUCTION	1
2	ORGANISATION	1
3	RISK MANAGEMENT IN THE PROJECT	1
4	DESCRIPTIONS OF EXPERIMENTAL SETUP.....	2
5	EVACUATION FROM THE EXPERIMENTAL AREA	3
6	WARNING	3
6.1	Before experiments.....	3
6.2	Non-conformance	3
7	ASSESSMENT OF TECHNICAL SAFETY	4
7.1	HAZOP.....	4
7.2	Flammable, reactive and pressurized substances and gas	4
7.3	Pressurized equipment.....	4
7.4	Effects on the environment (emissions, noise, temperature, vibration, smell)	4
7.5	Radiation	4
7.6	Chemicals.....	5
7.7	Electricity safety (deviations from the norms/standards)	5
8	ASSESSMENT OF OPERATIONAL SAFETY	5
8.1	Procedure HAZOP	5
8.2	Operation procedure and emergency shutdown procedure.....	5
8.3	Training of operators.....	5
8.4	Personal protective equipment.....	5
8.5	General Safety	5
8.6	Safety equipment	5
8.7	Special predations	5
9	QUANTIFYING OF RISK - RISK MATRIX.....	6

1 INTRODUCTION

The temperature response of a phase changing material will be measured in the test rig. A heat load will be applied to the system and temperatures and heat fluxes will be measured. The phase change material is Erythritol, it is nontoxic, and has a melting temperature of 120°C.

2 ORGANISATION

Rolle	
Prosjektleder	Erling Næss
Apparaturansvarlig	Erling Næss
Romansvarlig	Paul Svendsen
HMS koordinator	Morten Grønli
HMS ansvarlig (linjeleder):	Olav Bolland

3 RISK MANAGEMENT IN THE PROJECT

Hovedaktiviteter risikostyring	Nødvendige tiltak, dokumentasjon	DATE
Prosjekt initiering	Prosjekt initiering mal	
Veiledningsmøte Guidance Meeting	Skjema for Veiledningsmøte med pre-risikovurdering	
Innledende risikovurdering Initial Assessment	Fareidentifikasjon – HAZID Skjema grovanalyse	
Vurdering av teknisk sikkerhet Evaluation of technical security	Prosess-HAZOP Tekniske dokumentasjoner	
Vurdering av operasjonell sikkerhet Evaluation of operational safety	Prosedyre-HAZOP Opplæringsplan for operatører	
Sluttvurdering, kvalitetssikring Final assessment, quality assurance	Uavhengig kontroll Utstedelse av apparaturkort Utstedelse av forsøk pågår kort	

4 DESCRIPTIONS OF EXPERIMENTAL SETUP

The experimental setup is designed to give approximately 1D heat conduction in a phase change material. The phase change material will melt, and a melting front will move through the material.

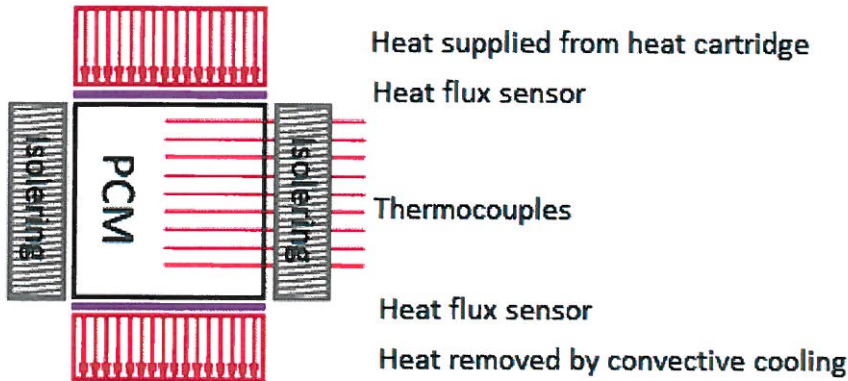


Figure 1 – General working principle (Heating from top)

The container holding the PCM is made out of Teflon, and is sealed using regular gaskets. The PCM will expand when melting and will flow from the main container to a heated expansion chamber. The flow path from the PCM container is next to the flux sensors as shown in Figure 2. When the PCM cools and solidifies, PCM will return from the expansion chamber to the main PCM chamber.

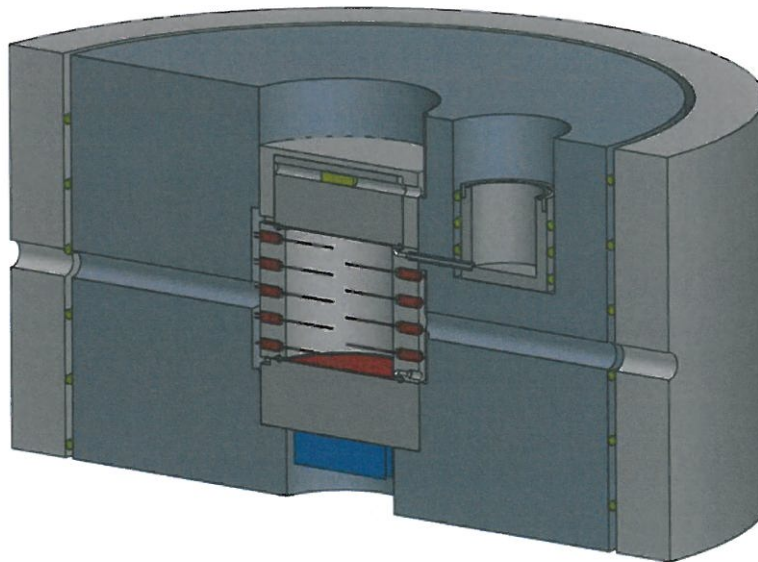


Figure 2 - Model of testrig with PCM container, end caps, heat spreader, flux sensors, heating elements and insulation visible.

There is no process to chart in a process diagram.

The instrumentation will include 2 heat flux transducers and around 20 thermocouples. Three sets of heating elements will be used; one for delivering heat for the experimental runs, one for insuring a temperature above the melting temperature in the expansion

chamber and one for limiting heat loss from the sides of the test rig. These heating elements will be regulated based on the measured temperatures and fluxes.

The logging and regulation will be done by a PC located next to the rig using Labview.

5 EVACUATION FROM THE EXPERIMENTAL AREA

Evacuate at signal from the alarm system or local gas alarms with its own local alert with sound and light outside the room in question, see 6.2

Evacuation from the rigging area takes place through the marked emergency exits to the assembly point, (corner of Old Chemistry Kjelhuset or parking 1a-b.)

Action on rig before evacuation:

The power to the rig should be turned off.

No negative reaction will occur because of this.

6 WARNING

6.1 Before experiments

Send an e-mail with information about the planned experiment to:

iept-experiments@ivt.ntnu.no

The e-mail must include the following information:

- Name of responsible person:
- Experimental setup/rig:
- Start Experiments: (date and time)
- Stop Experiments: (date and time)

You must get the approval back from the laboratory management before start up. All running experiments are notified in the activity calendar for the lab to be sure they are coordinated with other activity.

6.2 Non-conformance

FIRE

If you are NOT able to extinguish the fire, activate the nearest fire alarm and evacuate area. Be then available for fire brigade and building caretaker to detect fire place.

If possible, notify:

NTNU	SINTEF
Morten Grønli, Mob: 918 97 515	Harald Mæhlum, Mob: 930 14 986
Olav Bolland: Mob: 918 97 209	Anne Karin T. Hemmingsen Mob: 930 19 669
NTNU – SINTEF Beredskapstelefon	800 80 388

GAS ALARM

If a gas alarm occurs, close gas bottles immediately and ventilate the area. If the level of the gas concentration does not decrease within a reasonable time, activate the fire alarm and evacuate the lab. Designated personnel or fire department checks the leak to determine whether it is possible to seal the leak and ventilate the area in a responsible manner.

PERSONAL INJURY

- First aid kit in the fire / first aid stations
- Shout for help
- Start life-saving first aid
- **CALL 113** if there is any doubt whether there is a serious injury

OTHER NON-CONFORMANCE (AVVIK)

NTNU:

You will find the reporting form for non-conformance on:
<https://innsida.ntnu.no/wiki/-/wiki/Norsk/Melde+avvik>

SINTEF:

Synergi

7 ASSESSMENT OF TECHNICAL SAFETY

7.1 HAZOP

See Chapter 13 "Guide to the report template".

The experiment set up is divided into the following nodes:

Node 1	
Node 2	

Attachments, Form: Hazop_mal

Conclusion: (Safety taken care of)

7.2 Flammable, reactive and pressurized substances and gas

No flammable, reactive or pressurized gas in use.

7.3 Pressurized equipment

No pressurized equipment in use

7.4 Effects on the environment (emissions, noise, temperature, vibration, smell)

No effects on environment.

7.5 Radiation

No

7.6 Chemicals

No toxic chemicals will be used.

7.7 Electricity safety (deviations from the norms/standards)

No

8 ASSESSMENT OF OPERATIONAL SAFETY

Ensure that the procedures cover all identified risk factors that must be taken care of. Ensure that the operators and technical performance have sufficient expertise.

8.1 Procedure HAZOP

The method is a procedure to identify causes and sources of danger to operational problems.

Attachments:: HAZOP_MAL_Prosegyre

8.2 Operation procedure and emergency shutdown procedure

Attachments: Procedure for running experiments

8.3 Training of operators

Attachments: Training program for operators

8.4 Personal protective equipment

- *It is mandatory use of eye protection in the rig zone*

8.5 General Safety

- *Gas cylinders shall be placed in an approved carrier with shut-off valve within easy reach.*

8.6 Safety equipment

- *Warning signs, see the Regulations on Safety signs and signaling in the workplace*

8.7 Special predations

- NO

9 QUANTIFYING OF RISK - RISK MATRIX

The risk matrix will provide visualization and an overview of activity risks so that management and users get the most complete picture of risk factors.

IDnr	Aktivitet-hendelse	Frekv-Sans	Kons	RV
1	Readying rig for experiments: Melting the PCM requires temperatures up to 150°C. This may cause dangerous situations	1/2	A/B	B2
2	During experiments: Expansion can be hindered. This will cause leaks through the gaskets. These leaks can cause burns if touched.	1/2	A/B	B2

CONSEQUENCES	Catastrophic	E1	E2	E3	E4	E5
	Major	D1	D2	D3	D4	D5
	Moderate	C1	C2	C3	C4	C5
	Minor	B1	B2	B3	B4	B5
	Insignificant	A1	A2	A3	A4	A5
		Rare	Unlikely	Possible	Likely	Almost
		PROBABILITY				

Table 8. Risk's Matrix

Table 9. The principle of the acceptance criterion. Explanation of the colors used in the matrix

COLOUR	DESCRIPTION
Red	Unacceptable risk Action has to be taken to reduce risk
Yellow	Assessment area. Actions has to be considered
Green	Acceptable risk. Action can be taken based on other criteria

Attachment to Risk Assessment report

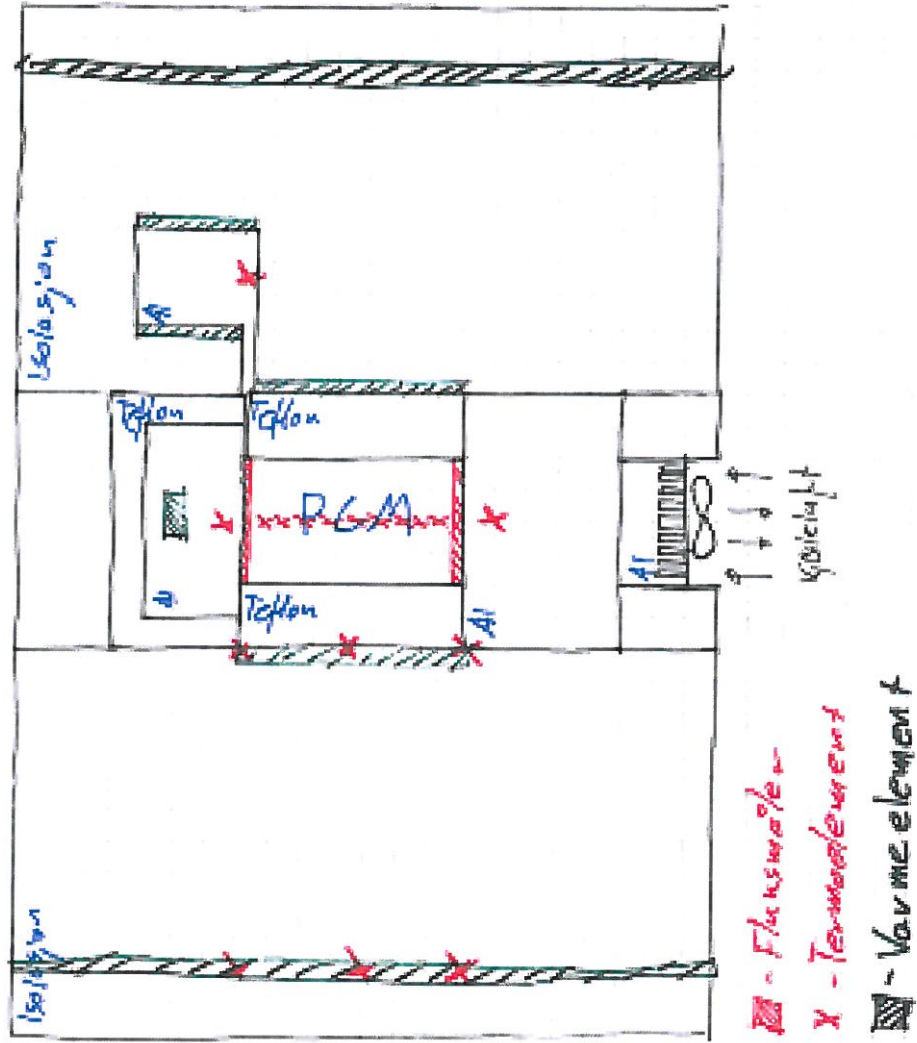
Stablewood- PCM Testtrigg

Prosjektnavn	Stablewood
Apparatur	PCM testtrigg
Enhet	NTNU-EPT
Apparaturansvarlig	Kolbeinn Kristjansson
Prosjektleder	Erling Næss
HMS-koordinator	Morten Grønli
HMS-ansvarlig (linjeleder)	Olav Bolland
Plassering	VATL
Romnummer	C165
Risikovurdering utført av	Kolbeinn Kristjansson

TABLE OF CONTENTS

ATTACHMENT A: PROCESS AND INSTRUMENTATION DIAGRAM	1
ATTACHMENT B: HAZOP	2
ATTACHMENT E: PROCEDURE FOR RUNNING EXPERIMENTS.....	3
ATTACHMENT F: TRAINING OF OPERATORS.....	5
APPARATURKORT / UNITCARD.....	6
FORSØK PÅGÅR /EXPERIMENT IN PROGRESS	7

ATTACHMENT A: PROCESS AND INSTRUMENTATION DIAGRAM



ATTACHMENT B: HAZOP

Project: Node: 1		Page					
Ref	Guideword	Causes	Consequences	Safeguards	Recommendations	Action	Date/Sign
	No flow	Blokkert ekspansjon	Lekkasje	Varmeelementer	-	-	-
	More pressure	"	"	"	-	-	-
	More temperature	Feil TC plassering/ Feil regulering	Ødelagt forsøk, mulig skade på teflon og varmeelement	God regulering og plassering av TC, sikker drift	-	-	-
	Service failure	PC-krasj	Se 'more temperature'	Bare kjøring med sikre varmelaster før man kjører med høy varmebelastning	-	-	-

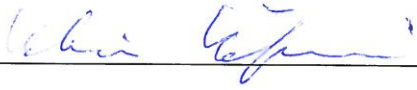
ATTACHMENT E: PROCEDURE FOR RUNNING EXPERIMENTS

Prosjekt Stablewood	Dato	Signatur
Apparatur PCM testtrigg		
Prosjektleder Erling Næss	2014-08-05	Erling Næss

	Conditions for the experiment:	Completed
	Experiments should be run in normal working hours, 08:00-16:00 during winter time and 08.00-15.00 during summer time. Experiments outside normal working hours shall be approved.	
	One person must always be present while running experiments, and should be approved as an experimental leader.	
	An early warning is given according to the lab rules, and accepted by authorized personnel.	
	Be sure that everyone taking part of the experiment is wearing the necessary protecting equipment and is aware of the shut down procedure and escape routes.	
	Preparations	Carried out
	Make sure there are no leaks, and that everything is properly aligned.	
	Make sure that the PCM level is high enough to ensure proper thermal contact. Refill if necessary.	
	Check that every instrument is functioning and positioned properly.	
	Check that every heating element is functioning properly	
	Check the condition on the cold side of the rig. Adjust fan speed and or depth of insulation.	
	Start up procedure	
	<i>Insert experimental paramaters into LABview (Regulation for the heating element, ie temperature or flux)</i>	
	<i>Start the heating (Make sure expansion tank heating elements are working)</i>	
	During the experiment	
	<i>Inspect temperatures and fluxes regularly</i>	
	End of experiment	
	<i>Increase cooling, solidification has to happen from the bottom of the tank.</i>	
	<i>Shut of experimental heating, but maintain a liquid state in the expansion chamber to ensure proper reflux of fluid.</i>	
	Turn of expansion chamber heating after the reflux is finished.	
	Remove all obstructions/barriers/signs around the experiment.	
	Tidy up and return all tools and equipment.	
	Tidy and cleanup work areas.	
	Return equipment and systems back to their normal operation settings (fire alarm)	
	To reflect on before the next experiment and experience useful for others	
	Was the experiment completed as planned and on scheduled in professional terms?	

	Was the competence which was needed for security and completion of the experiment available to you?	
	Do you have any information/ knowledge from the experiment that you should document and share with fellow colleagues?	

Operator(s):

Navn	Dato	Signatur
Kolbeinn Kristjansson		

ATTACHMENT F: TRAINING OF OPERATORS

Prosjekt	Dato	Signatur
Stablewood		
Apparatur PCM testtrigg		
Prosjektleder Erling Næss	2014-08-13	E. Næss

Knowledge about EPT LAB in general	
Lab	
<ul style="list-style-type: none"> • Access • routines and rules • working hour 	
Knowledge about the evacuation procedures.	
Activity calendar for the Lab	
Early warning, iept-experiments@ivt.ntnu.no	
Knowledge about the experiments	
Procedures for the experiments	
Emergency shutdown.	
Nearest fire and first aid station.	

I hereby declare that I have read and understood the regulatory requirements has received appropriate training to run this experiment and are aware of my personal responsibility by working in EPT laboratories.

Operator(s):

Navn	Dato	Signatur
Kolbeinn Kristjansson		Kolbeinn Kristjansson

APPARATURKORT / UNITCARD

Dette kortet SKAL henges godt synlig på apparaturen!
This card MUST be posted on a visible place on the unit!

Apparatur (Unit) PCM testrigg	
Prosjektleder (Project Leader) Erling Næss	Telefon mobil/privat (Phone no. mobile/private)
Apparaturansvarlig (Unit Responsible) Kolbeinn Kristjansson	Telefon mobil/privat (Phone no. mobile/private)
Sikkerhetsrisikoer (Safety hazards)	
Sikkerhetsregler (Safety rules) Use safety googles	
Nødstop prosedyre (Emergency shutdown) Turn off the power supply	

Her finner du (Here you will find):

Prosedyrer (Procedures)	aaa
Bruksanvisning (Users manual)	bbb

Nærmeste (Nearest)

Brannslukningsapparat (fire extinguisher)	aaaa
Førstehjelpsskap (first aid cabinet)	bbbb

NTNU
Institutt for energi og prosessteknikk

Dato

Signert

FORSØK PÅGÅR / EXPERIMENT IN PROGRESS

Dette kortet SKAL henges opp før forsøk kan starte!
This card MUST be posted on the unit before the experiment startup!

Apparatur (Unit) PCM testtrigg	
Prosjektleder (Project Leader) Erling Næss	Telefon mobil/privat (Phone no. mobile/private)
Apparaturansvarlig (Unit Responsible) Kolbeinn Kristjansson	Telefon mobil/privat (Phone no. mobile/private)
Godkjente operatører (Approved Operators) Kolbeinn Kristjansson	Telefon mobil/privat (Phone no. mobile/private)
Prosjekt (Project) Stablewood	
Forsøks tid / Experimental time (start - stop)	
Kort beskrivelse av forsøket og relaterte farer (Short description of the experiment and related hazards) The temperature response of a phase changing material will be measured in the test rig. A heat load will be applied to the system and temperatures and heat fluxes will be measured. The phase change material is Erythritol, it is nontoxic, and has a melting temperature of 120°C.	

NTNU
Institutt for energi og prosessteknikk

Dato

Signert
